## T CELLS

# 3D chromatin reprogramming primes human memory T$_H$2 cells for rapid recall and pathogenic dysfunction

Anne Onrust-van Schoonhoven[1,2], Marjolein J.W. de Bruijn[1], Bernard Stikker[1], Rutger W.W. Brouwer[3], Gert-Jan Braunstahl[1,4], Wilfred F.J. van IJcken[3], Thomas Graf[5,6], Danny Huylebroeck[2], Rudi W. Hendriks[1], Grégoire Stik[7]*, Ralph Stadhouders[1,2]*

Memory T cells provide long-lasting defense responses through their ability to rapidly reactivate, but how they efficiently "recall" an inflammatory transcriptional program remains unclear. Here, we show that human CD4$^+$ memory T helper 2 (T$_H$2) cells carry a chromatin landscape synergistically reprogrammed at both one-dimensional (1D) and 3D levels to accommodate recall responses, which is absent in naive T cells. In memory T$_H$2 cells, recall genes were epigenetically primed through the maintenance of transcription-permissive chromatin at distal (super)enhancers organized in long-range 3D chromatin hubs. Precise transcriptional control of key recall genes occurred inside dedicated topologically associating domains ("memory TADs"), in which activation-associated promoter-enhancer interactions were preformed and exploited by AP-1 transcription factors to promote rapid transcriptional induction. Resting memory T$_H$2 cells from patients with asthma showed premature activation of primed recall circuits, linking aberrant transcriptional control of recall responses to chronic inflammation. Together, our results implicate stable multiscale reprogramming of chromatin organization as a key mechanism underlying immunological memory and dysfunction in T cells.

## INTRODUCTION

T lymphocytes use a near-infinite repertoire of antigen-specific receptors to generate adaptive immune responses against pathogens and malignant cells (*1*). CD4$^+$ T helper (T$_H$) cell subsets orchestrate adaptive immunity through the production of specialized cytokines (*2*): T$_H$1 cells produce interferon-γ (IFN-γ) to combat intracellular bacteria and viruses; T$_H$2 cells secrete interleukin-4 (IL-4), IL-5, IL-9, and IL-13 to expel parasites; and T$_H$17 cells synthesize IL-17 to defend against extracellular bacteria or fungi. During T cell responses, a fraction of activated cells adopt a memory phenotype and return to quiescence. These long-lived memory T cells retain an irreversible molecular imprint that enables them to mount a secondary recall response to the same antigen faster and greater in magnitude than the primary response of a naive cell (*3*). Memory T cells thus provide long-lasting immunological protection, forming the foundation for vaccination strategies (*4*). Moreover, pathogenic dysfunction of memory T cells has been implicated in major diseases, including autoimmunity [T$_H$17 cells (*5*)] and asthma [T$_H$2 cells (*6*, *7*)].

Functionally distinct cellular states and phenotypes emerge from specific gene expression programs, which are controlled at the epigenomic level. Epigenomes consist of one-dimensional (1D) features such as chromatin accessibility and posttranslational histone modifications that either facilitate or impede access of DNA binding transcription factors (TFs) to gene regulatory elements such as promoters and enhancers (*8*, *9*). Epigenomes adopt a nonrandom 3D organization of chromatin that is tightly linked to the control of gene expression (*10*–*14*). Examples include clustering of genomic regions with similar levels of transcriptional activity in chromosome compartments (i.e., active genes tend to reside in the so-called A compartment, repressed genes in the B compartment), the formation of spatially insulated genomic neighborhoods called topologically associating domains (TADs), and enhancer-promoter interactions preferentially occurring within these TADs.

Human T cell activation involves coordinated changes in 1D and 3D chromatin structure as well as gene expression (*15*–*22*), resulting in phenotypic changes characterized by metabolic reprogramming and inflammatory cytokine production. Memory T cells have a distinct transcriptome and epigenome as compared with their naive counterparts (*15*, *16*, *23*–*29*), indicating that the molecular basis of the memory T cell response is anchored in mechanisms of transcriptional control (*30*). Whereas priming of the chromatin landscape in resting memory cells has been implicated in facilitating rapid recall (*27*, *28*, *31*–*33*), we still lack detailed insight into the epigenomic circuitry that endows human memory T cells with their ability to rapidly activate specific sets of inflammatory genes. Furthermore, the role of 3D genome conformation for T cell memory has not been systematically addressed (*22*). Here, we applied a multiscale 1D/3D epigenomic approach to comprehensively dissect the molecular program driving rapid recall in primary human memory T$_H$2 cells. Our analyses reveal functionally distinct epigenomic priming mechanisms underlying rapid recall, which are stably stored in memory T cells at the level of transcription, chromatin accessibility, and 3D genome folding. We also find that this distinct reprogramming of 1D/3D chromatin organization in memory T$_H$ cells is exploited by AP-1 TFs for efficient transcriptional reactivation and is dysregulated in resting memory T$_H$2 cells from patients with asthma.

[1]Department of Pulmonary Medicine, Erasmus MC, University Medical Center Rotterdam, Rotterdam, Netherlands. [2]Department of Cell Biology, Erasmus MC, University Medical Center Rotterdam, Rotterdam, Netherlands. [3]Center for Biomics, Erasmus MC, University Medical Center Rotterdam, Rotterdam, Netherlands. [4]Department of Respiratory Medicine, Franciscus Gasthuis and Vlietland, Rotterdam, Netherlands. [5]Centre for Genomic Regulation (CRG) and Institute of Science and Technology (BIST), Barcelona, Spain. [6]Universitat Pompeu Fabra (UPF), Barcelona, Spain. [7]Josep Carreras Leukaemia Research Institute (IJC), Badalona, Spain.
*Corresponding author. Email: r.stadhouders@erasmusmc.nl (R.S.); gstik@carreras-research.org (G.S.)

## RESULTS

### An experimental system to identify epigenomic drivers of T cell memory

To systematically identify epigenomic mechanisms underlying rapid recall in memory T cells, we interrogated gene expression, chromatin structure, and 3D genome conformation dynamics during early memory T cell activation (Fig. 1, A and B). Contrasting memory and naive T cells allows for separation of events that are specific to memory T cell activation from those that are shared with naive cells that lack memory of a prior stimulation. We focused on naive CD4$^+$ T cells (CD4$^+$CD127$^+$CD25$^-$CD45RA$^+$) and memory T$_H$2 cells (CD4$^+$CD127$^+$CD25$^-$CD45RA$^-$CCR6$^-$CXCR3$^-$CXCR5$^-$CCR4$^+$) isolated using fluorescence-activated cell sorting (FACS) from peripheral blood samples of healthy donors (Fig. 1C). T cells were either analyzed as resting, unstimulated cells ("−") or stimulated in vitro for 24 hours using bead-linked anti-CD3/CD28 antibodies ("+") to activate T cell receptor (TCR) signaling and costimulatory pathways.

Gene expression was measured by RNA-sequencing (RNA-Seq), and genome-wide 3D chromosome conformation was assessed using in situ Hi-C; chromatin accessibility information was obtained from available assay for transposase-accessible chromatin using sequencing (ATAC-Seq) data from precisely matched T cell populations (15). Examining expression levels of signature T$_H$ cell cytokines revealed a strong and reproducible induction of canonical T$_H$2 cytokine genes (e.g., IL4 and IL5) in memory T$_H$2 cells, whereas signature T$_H$1/T$_H$17 genes (e.g., IFNG and IL17A) remained silent (Fig. 1D and fig. S1A). Conversely, activated naive CD4$^+$ T cells only produced IFNG mRNA and showed virtually undetectable T$_H$2 cytokine gene expression (Fig. 1D and fig. S1A), confirming that our experimental setup accurately and reproducibly captures the recall ability of memory T$_H$2 cells.

### Transcriptional modules linked to rapid recall in CD4$^+$ memory T cells

Differential gene expression analysis revealed widespread transcriptional changes after 24 hours of stimulation, including well-known markers of T cell activation such as IL2RA (encoding the high-affinity IL-2 receptor subunit CD25) and MYC (fig. S1B). Although naive CD4$^+$ T cells lack any recall ability, they showed a quantitatively and qualitatively similar transcriptional response to stimulation as memory T$_H$2 cells, i.e., 7997 and 7368 differentially expressed genes, respectively, of which ~80% were shared between naive and memory cells (Fig. 1E and fig. S1, C and D). Thus, large-scale transcriptional rewiring shortly after activation is highly comparable in naive and memory CD4$^+$ T cells, suggesting that the transcriptional program associated with memory recall consists of a restricted number of genes.

Previous studies have detected hundreds of differentially expressed genes between naive and memory T cells (30). They, however, did not investigate recall-associated transcriptional activation, which we define here as stimulation-induced genes that show increased expression in memory T cells compared with naive T cells before and/or upon early activation ("recall genes"). To identify recall genes, we used several clustering and filtering strategies (see Methods and fig. S1, E and F). Of the 742 differentially expressed genes between resting naive CD4$^+$ T cells and resting memory T$_H$2 cells (fig. S1, C and D), we extracted 150 stimulation-induced genes that were already up-regulated in resting memory T$_H$2 versus resting naive CD4$^+$ T cells and that were further induced upon T cell activation (recall module I; Fig. 1F and fig. S1E). Pathway enrichment analyses revealed that these genes were functionally involved in glycolytic metabolism (e.g., GAPDH and PGK1), lymphocyte activation (e.g., CD58 and IL2), apical protein localization (e.g., RAB8B), and cytoskeletal organization (e.g., ACTB and RHOG) (Fig. 1G). Earlier work provided evidence that memory T cells exhibit elevated glycolysis and increased cortical actin content to facilitate rapid recall (34, 35), validating our experimental approach. In addition, we identified several genes encoding molecules not previously implicated in T$_H$ cell recall, including the long noncoding RNA CYTOR, the C-type lectin-like receptor CLECL1, the histone 3 lysine 27 (H3K27) methyltransferase EZH2, and several AP-1 family TFs (i.e., BATF, FOSL2, and CREM).

Clustering of all stimulation-induced genes in both cell types revealed two additional modules of recall genes that showed similar expression in both resting T cell subsets but are poised for more rapid reactivation in memory T$_H$2 cells (recall modules II and III; Fig. 1F and fig. S1F). Module II consists of 230 genes strongly induced only in activated memory T$_H$2 cells, whereas module III genes ($n = 504$) were up-regulated in both cell types but substantially higher in memory T$_H$2 cells (Fig. 1F). Module II genes showed higher overall inducibility than module III genes (average: 3.7 versus 2.4 log$_2$ fold change, respectively) (fig. S1G). Recall module II genes were poorly expressed in resting memory cells [median level of 1.1 reads per kilobase per million (RPKM)] and encoded all canonical T$_H$2 cytokines as well as critical immunomodulatory molecules (e.g., ICOS and CTLA4). Module III genes were enriched for more diverse yet highly relevant biological functions, which included cell cycle control (e.g., CDK5), lipid metabolism (e.g., ACOX1), and lymphocyte activation (e.g., IL2RA, IRF4, and SLAMF1) (Fig. 1, F and G). Network analysis of enriched biological pathways revealed that the three recall gene modules (data file S1) were to a large extent functionally interconnected (Fig. 1H). Flow cytometry analyses confirmed similar dynamics of selected factors from the three modules at the protein level (Fig. 1I). All three recall gene modules showed similar expression dynamics in resting and activated memory T$_H$1 or T$_H$17 cells (fig. S1H) (15), indicating that they are shared across CD4$^+$ memory T cell subsets. Applying an additional set of stringent filtering criteria identified recall genes with T$_H$2-specific activation dynamics ($n = 27$, see Methods), but many more showed stronger induction in all three T$_H$ subsets as compared with naive cells ("T$_H$-shared" recall genes, $n = 199$) (fig. S1I).

Last, we also defined genes associated with transcriptional silencing upon T cell stimulation and that show decreased expression in memory T$_H$2 cells compared with naive T cells before and/or upon early activation. Four clusters of such "inverse recall" genes emerged ($n = 281$ genes in total), all showing lower expression already at baseline in memory T$_H$2 cells (fig. S2, A and B). These genes were enriched in biological pathways relevant for T cell biology, including known regulators of T cell stemness, homeostatic proliferation, and metabolic reprogramming such as BACH2, TCF7, and LEF1 (fig. S2C).

Together, these results show that resting memory CD4$^+$ T$_H$2 cells maintain increased expression of a highly restricted set of stimulation-induced genes (recall module I). These do not include prototypical regulators of T$_H$2 cell effector function, which are instead

**Fig. 1. Identification of distinct transcriptional modules linked to rapid recall in human CD4+ memory T cells.** (**A**) Potential epigenomic drivers of rapid recall investigated in this study. (**B**) Experimental system used to investigate the epigenomic underpinnings of rapid transcriptional recall in human memory ("mem.") $T_H2$ cells. Cells were stimulated with bead-linked anti-CD3 and anti-CD28 antibodies to mimic generic TCR and CD28 co-receptor activation. (**C**) Flow cytometry gating strategy used to isolate human naive CD4+ T cells and memory $T_H2$ cells from peripheral blood. (**D**) mRNA expression levels of signature $T_H$ cytokine genes in the indicated resting (−) and stimulated (+) cells. Data represent measurements from three independent biological replicates. (**E**) PCA of scaled gene expression values for all genes expressed in at least one sample type ($n = 12,284$ genes). (**F**) Heatmap showing mRNA expression levels for genes within three recall-associated gene modules (example genes are indicated). Boxplots on the right indicate averaged expression values (z-score scaled) for each module in each of the four indicated T cell samples. $P$ values: Kruskal-Wallis test corrected for multiple testing. ns, not significant. (**G**) Pathway enrichment analysis of genes belonging to the three modules. GTPases, guanosine triphosphatases; ER, endoplasmic reticulum; JAK, Janus kinase. (**H**) Network of biological pathways associated with recall-associated module genes. Nodes represent individual pathways ($P < 0.05$) that are connected and clustered on the basis of functional similarity. Nodes are represented as pie charts: The size of a pie is proportional to the total number of hits; pie charts are color-coded on the basis of the module origin of the associated genes. Circos plot indicates connections between the three modules at the pathway level, with gray lines linking genes that belong to the same enriched pathway. (**I**) mRNA gene expression (top) and protein levels (as measured by flow cytometry, bottom) of selected module members.
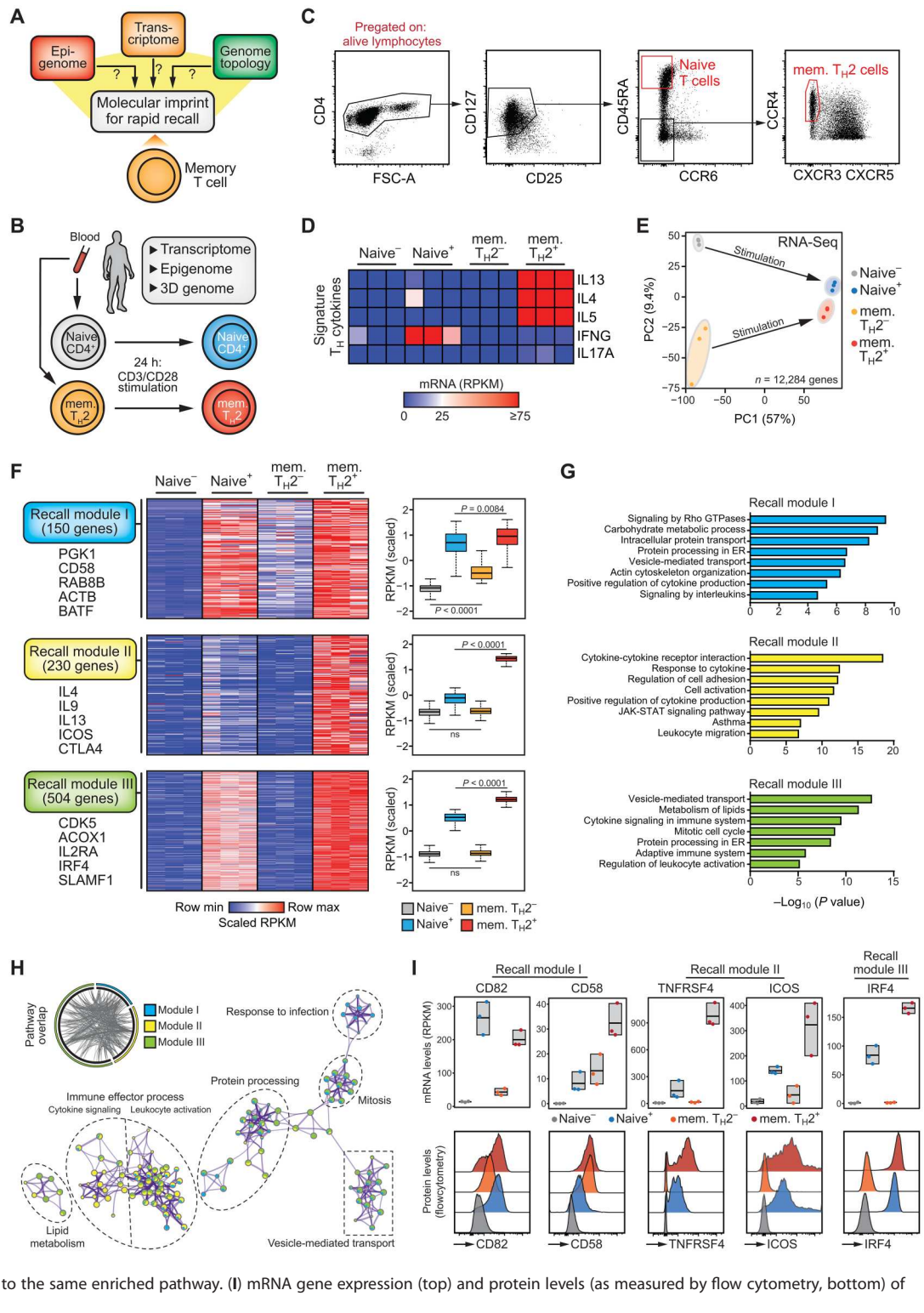
organized in two larger recall gene modules (II and III) that show no differential expression at baseline but are more robustly induced upon TCR stimulation in memory $T_H$ cells as compared with naive $T_H$ cells. In addition, a small number of stimulation-repressed genes encoding for regulators of T cell homeostasis are expressed at lower levels in memory $T_H2$ cells, many of which are silenced more efficiently in memory cells upon activation.

## Extensive epigenomic priming of effector loci in resting memory $T_H$ cells

Chromatin accessibility landscapes analyzed using ATAC-Seq can be exploited to identify potential regulators of transcriptional programs underlying specific immune cell states (*15*, *24*, *36*). In line with transcriptional changes, both naive CD4$^+$ T cells and memory $T_H1$, $T_H2$, and $T_H17$ cells showed similar capacities for rapid genome-wide expansion of chromatin accessibility (~2-fold increase in total ATAC-Seq peaks; fig. S3, A and B). Principal components analysis (PCA) not only confirmed the major effect of stimulation on the epigenome but also separated resting naive from memory T cells (Fig. 2A). Clustering of differentially accessible sites across all cell states (*n* = 32,847 peaks, see Methods) revealed various patterns of ATAC-Seq signal dynamics, including several clusters of naive-specific peaks (Fig. 2B and fig. S3, C and D).

We detected several clusters of sites that either were uniquely present in memory $T_H$ cells—irrespective of stimulation status—or gained chromatin accessibility upon stimulation and were already accessible in resting memory $T_H2$ cells. We refer to these clusters shared across all memory $T_H$ subsets (memory-specific) or specific to $T_H2$ cells as "recall-associated" accessible chromatin regions (*n* = 3025 peaks in total) (Fig. 2B and fig. S3, C and D). Recall-associated accessible chromatin was predominantly (88.9%) localized to distal regulatory elements and linked to genes enriched for effector cell–associated functions such as lymphocyte activation, cytokine production, and cell adhesion (Fig. 2, C and D, and fig. S3E). A substantial fraction of genes from the three recall modules (22 to 44%; *P* < 0.0001, Fisher's exact test) was associated with a stimulation-induced ATAC-Seq peak already present in resting $T_H$ memory cells, as exemplified by *IL3* (Fig. 2, E and F). Similar results were obtained when using $T_H2$-specific and $T_H$-shared recall gene definitions (27 and 78%, respectively; *P* < 0.0001) (fig. S3F). A small group of $T_H$-shared recall genes with critical roles in memory T cell activation (e.g., *IRF4*, *ICOS*, and *MAF*) showed epigenomic priming in both a $T_H$-shared and a $T_H2$-specific fashion (fig. S3F), indicating that memory $T_H$ cells may use a combination of shared and subset-specific regulatory elements to facilitate rapid gene induction. Using additional stringent filtering criteria (see Methods), we identified 130 genes that were primed at the level of chromatin accessibility in resting memory cells and had a significant expression advantage specifically after stimulation. These included genes encoding key inflammatory cytokines (e.g., *IL3*, *IL9*, and *IL13*), costimulatory molecules (e.g., *ICOS*, *OX40*, and *GITR*), the high-affinity IL-2 receptor subunit (*IL2RA*), and the MAF AP-1 family TF (Fig. 2G). Around 46% (*P* < 0.0001, Fisher's exact test) of stimulation-repressed inverse recall genes could be linked to ATAC-Seq peaks that were uniquely present in naive $T_H$ cells (fig. S2D; using the "naive-specific" clusters from fig. S3C).

Specific chromatin features have previously been associated with epigenomically primed (or "poised") loci (*37*, *38*), including H3K4

dimethylation (H3K4Me2), H3K27Me3, RNA polymerase II (RNAPII), and the H2A.Z histone variant. Conversely, these regions are generally low in H3K27Ac, a hallmark of transcriptional activity (*37*). We profiled H3K4Me2 in resting naive or memory CD4$^+$ T cells from three independent donors using ChIPmentation (*39*) and obtained H3K27Me3, RNAPII, H2A.Z, and H3K27Ac chromatin immunoprecipitation followed by high-throughput sequencing (ChIP-Seq) data from published studies (see Methods). In line with bona fide priming, stimulation-induced regions accessible in resting memory $T_H$ cells showed low levels of H3K27Ac [obtained from total $T_H$ memory cells (*40*)], which increased upon activation (Fig. 3A and fig. S4, A and B). In contrast, H3K27Ac levels at naive-specific ATAC-Seq peaks were not induced after stimulation of memory $T_H$ cells (Fig. 3A). Recall-associated accessible chromatin showed no enrichment for H3K27Me3 and was marked by H2A.Z in both naive and memory CD4$^+$ T cells (fig. S4, C and D). However, we observed strong and specific enrichment for H3K4Me2 and RNAPII at these sites in memory cell subsets compared with naive cells (Fig. 3, B and C, and fig. S4E).

We next conducted motif enrichment analysis to identify TFs associated with recall-associated chromatin priming in memory CD4$^+$ T cells. Whereas naive-specific accessible chromatin was enriched for CTCF and TCF factor motifs (fig. S4F) (*41*), all three memory-specific clusters were strongly enriched for AP-1, RUNX, and ETS family motifs (Fig. 3D). The $T_H2$-specific cluster was uniquely enriched for GATA alongside RUNX and ETS motifs (Fig. 3D), in line with an important role for the $T_H2$ lineage–determining TF GATA3 (*42*) at these sites. RNA-Seq revealed that nine members from the AP-1, RUNX, or ETS TF families were up-regulated in resting or stimulated $T_H2$ cells compared with naive cells (Fig. 3E and fig. S4G), compatible with roles in maintaining recall-associated chromatin priming (e.g., *BATF*, *FOSL2*, and *RUNX3*) and/or in exploiting these sites once memory $T_H2$ cells are activated (e.g., *BATF3*, *MAF*, and *ETV6*). ChIP-Seq experiments (*43*, *44*) revealed extensive binding of GATA3 and in particular AP-1 TFs (i.e., 50% of all sites) at recall-associated accessible chromatin sites in activated memory $T_H$ cells (Fig. 3F). To test the functional relevance of AP-1 family TFs for recall, we treated memory $T_H2$ cells with a selective small-molecule inhibitor of AP-1 TF binding [T-5224 (*45*)] before stimulation. Treatment with T-5224 blunted transcriptional recall of selected recall genes (i.e., *IL4* and *IL5*), whereas the effect on early induction of general T cell activation markers *HPRT* and *CD40LG* was limited (Fig. 3G). We next used CRISPR-Cas9 genome editing in resting memory $T_H2$ cells to mutate the coding sequence of the *MAF* gene, encoding an AP-1 family TF implicated in $T_H2$ specification (*46*). Ribonucleoprotein complexes of Cas9 and guide RNAs successfully abrogated MAF protein production (Fig. 3H), blunting transcriptional recall of several type 2 cytokine genes but not the early induction of general stimulation-responsive genes (Fig. 3I and fig. S4H).

In summary, resting memory CD4$^+$ T cells carry a defined set of epigenomically primed gene regulatory elements that mark a restricted set of genes for rapid recall. Upon activation, these "recall enhancers" are targeted by lineage-determining (e.g., GATA3) and signal-responsive TFs (e.g., the AP-1 factor MAF) to enable robust induction of inflammatory gene expression.
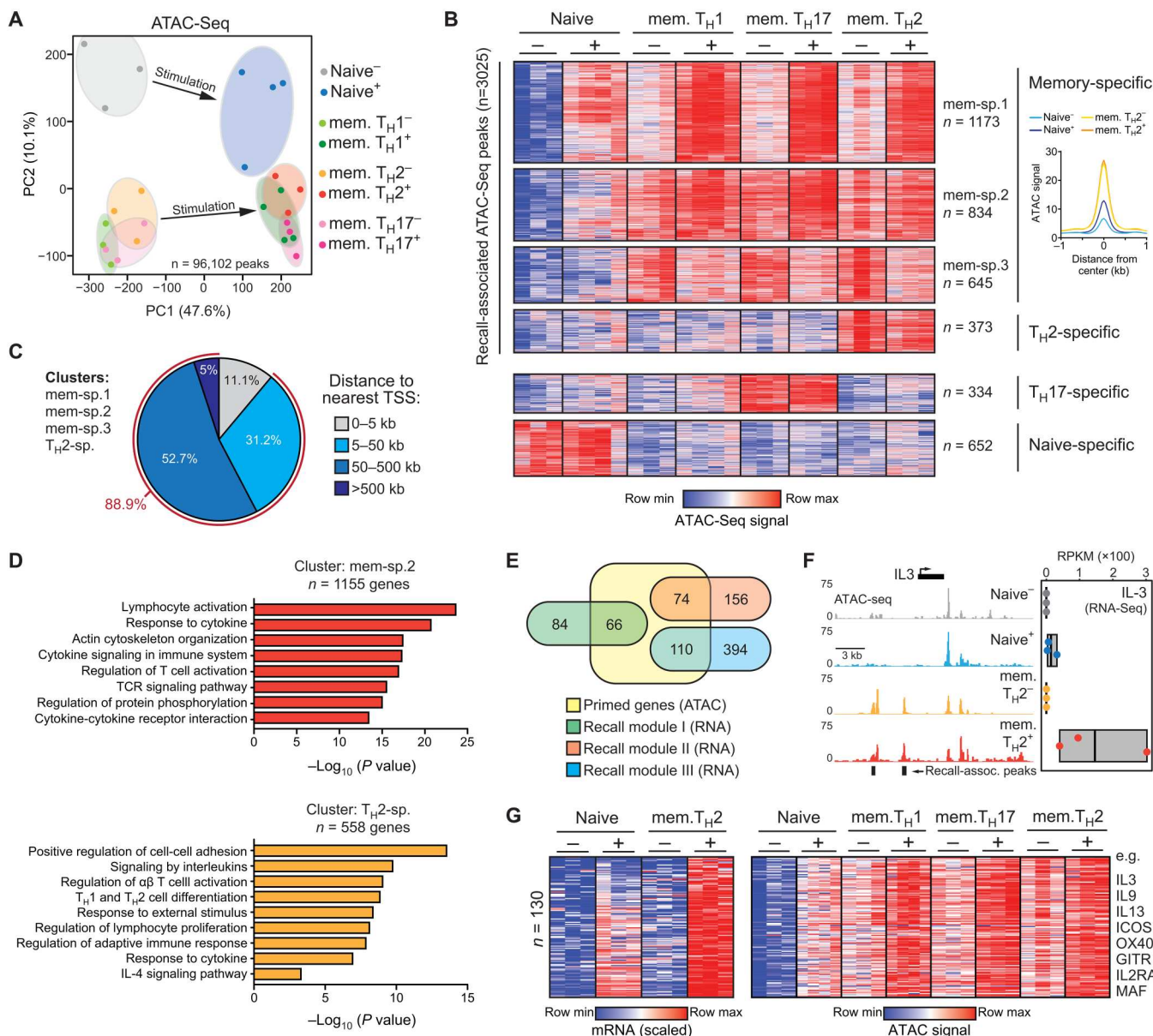
**Fig. 2. Extensive priming of chromatin accessibility in resting human CD4+ memory T cells.** (**A**) PCA of normalized accessibility values for all reproducibly detected ATAC-Seq peaks (present in at least one sample type, $n = 96,102$ peaks). (**B**) Heatmap showing normalized ATAC-Seq signals of indicated peak clusters in the indicated resting (−) and stimulated (+) cells. Line graph indicates averaged signal across all peaks within the three memory-specific clusters. (**C**) Pie chart depicting distances of recall-associated ATAC-Seq cluster peaks in human $T_H2$ cells to the nearest transcription start site (TSS). Red line indicates proportion of peaks outside of promoter regions. (**D**) Pathway enrichment analysis of genes closest to ATAC-Seq peaks from the indicated clusters. (**E**) Overlap between genes linked to recall-associated ATAC-Seq peaks ("Primed genes") and genes from the three recall-associated transcriptional modules (see Fig. 1). (**F**) Genome browser screenshot showing ATAC-Seq profiles at the primed *IL3* locus in resting (−) and stimulated (+) naive or memory $T_H2$ cells. Boxplot depicts *IL3* mRNA levels in samples from three independent donors. (**G**) Heatmaps with RNA-Seq (left) and ATAC-Seq (right) signals across the indicated sample types for epigenomically primed genes with a statistically significant expression advantage after stimulation. Example genes are indicated.

## Chromatin priming is linked to superenhancer modules

Superenhancers have emerged as clusters of multiple regulatory elements that ensure robust expression of key cell identity genes (*9*). We defined superenhancers in naive and memory $T_H2$ cells on the basis of H3K4Me2 abundance (*47*) to detect both active and primed superenhancer elements in resting T cells. H3K4Me2 superenhancer–associated genes in $T_H2$ memory cells were robustly expressed (>3-fold higher than the average expressed gene) and included signature T cell genes such as *BCL11B*, *CD3E*, and *IL7R* (fig. S4I). Compared with naive CD4+ T cells, resting $T_H2$ memory cells showed an expanded superenhancer landscape (1.8-fold more superenhancers; fig. S4I). Stringent filtering (>2-fold H3K4Me2 enrichment versus naive CD4+ T cells) yielded 83 $T_H2$ memory–specific superenhancers associated with 80 unique genes, which are
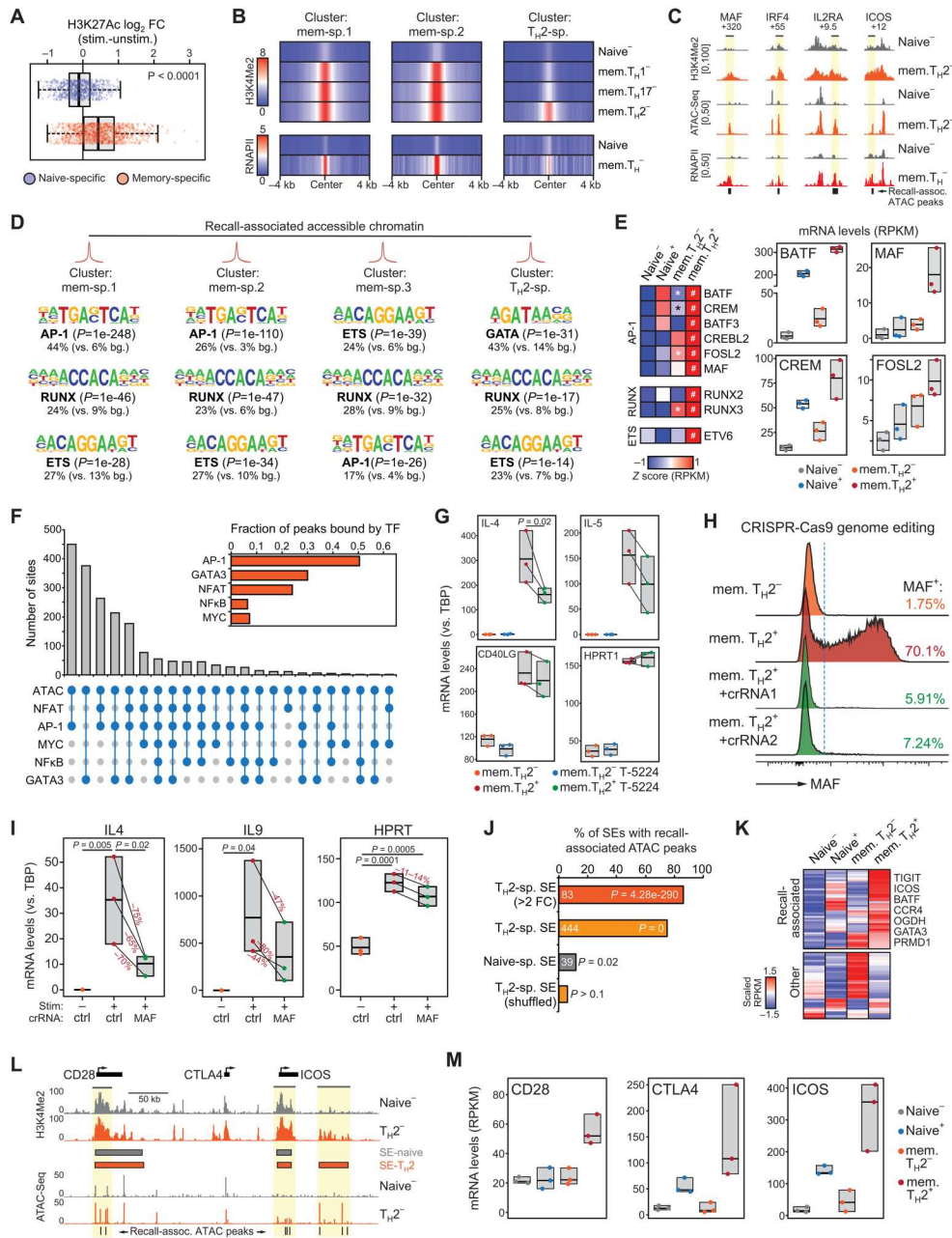
**Fig. 3. Specific TFs govern the recall-associated chromatin landscape in human CD4+ memory T cells.** (**A**) Fold changes (log$_2$ scale) in H3K27Ac levels upon TCR stimulation of total CD4+ memory T cells for naive-specific ($n$ = 652) or recall-associated (mem-sp.1 cluster, $n$ = 1173) ATAC-Seq peaks. (**B**) Heatmap representations of averaged H3K4Me2 (top) or RNA polymerase II (RNAPII, bottom) ChIP-Seq signal at the indicated recall-associated ATAC-Seq peak clusters in different resting T cell subsets. (**C**) Genome browser screenshots showing H3K4Me2, ATAC, and RNAPII signals at selected recall-associated ATAC-Seq peaks. Numbers on top indicate distance to TSS in kilobase. (**D**) Top three overrepresented TF binding motifs based on $P$ values for the indicated recall-associated ATAC-Seq peak clusters. Percentages indicate proportion of sites in which motif was detected [versus background (vs. bg.)]. (**E**) Scaled mRNA levels ($z$-score) of motif-associated TF genes significantly up-regulated in memory T$_H$2 cells compared with naive CD4+ T cells, either at resting state (*$P$ < 0.05) or after activation (#$P$ < 0.05). Boxplots depict RPKM values of selected genes from the heatmap. (**F**) TF occupancy patterns at all recall-associated ATAC-Seq peaks ($n$ = 3025 peaks) in stimulated CD4+ memory T cells. Inset bar graph shows total fraction of peaks bound the indicated TF. (**G**) Expression analysis of recall (*IL4* and *IL5*) and general activation (*CD40LG* and *HPRT*) genes in resting (−) and stimulated (+) memory T$_H$2 cells with or without T-5224 AP-1 inhibitor before treatment ($n$ = 3 independent biological replicates). (**H**) Flow cytometry analysis of MAF protein levels in resting (−) and stimulated (+) memory T$_H$2 cells. Bottom two tracks show cells in which *MAF* was disrupted using CRISPR-Cas9 with two different crRNAs, preventing MAF induction. (**I**) Expression analysis of recall (*IL4* and *IL9*) and general activation (*HPRT*) genes in resting (−) and stimulated (+) memory T$_H$2 cells pretreated with Cas9 and a nontargeting control (ctrl) or *MAF* crRNA. (**J**) Proportion of indicated superenhancer (SE) categories that overlap with recall-associated ATAC-Seq peaks, including $P$ values indicating statistical significance of the overlaps shown. (**K**) Heatmap showing mRNA expression levels for genes linked to memory T$_H$2-specific SEs (example genes are indicated). (**L**) Genome browser screenshot (top: H3K4Me2 ChIPmentation, bottom: ATAC-Seq) of the SE landscape at the *CD28-CTLA4-ICOS* locus. (**M**) Boxplots depicting gene expression dynamics of *CD28*, *CTLA4*, and *ICOS*. Statistical tests used: (A, G, and I) Mann-Whitney $U$ test; (D and J) Fisher's exact test; (E) DESeq2 Wald test.

involved in critical processes linked to memory T cell function. These included enhanced mitochondrial respiration (e.g., *OGDH*), migratory capacity (e.g., *CCR4*), activation (e.g., *ICOS* and *TIGIT*), and $T_H2$ cell identity (e.g., *GATA3* and *PRMD1*) (fig. S4J).

More than 80% of $T_H2$-specific superenhancers colocalized with recall-associated ATAC-Seq peaks (versus 11% for naive-specific superenhancers; $P < 0.0001$, Fisher's exact test), revealing widespread chromatin priming at superenhancers in resting memory $T_H$ cells (Fig. 3J and fig. S4K). Many $T_H2$-specific superenhancer-associated genes showed recall-associated transcriptional dynamics (Fig. 3K and fig. S4L). This is illustrated by the *CD28-CTLA4-ICOS* locus encoding three surface receptors that control T cell activity (*48*). Several superenhancers already established in resting memory $T_H2$ cells, including a $T_H2$-specific one downstream of *ICOS*, show increased accessibility at stimulation-associated open chromatin sites specifically in resting $T_H2$ cells (Fig. 3L). In accordance with transcriptional priming in memory cells, TCR stimulation more efficiently induced *CD28-CTLA4-ICOS* expression in $T_H2$ cells (Fig. 3M). Collectively, these results indicate that primed superenhancers control the activation-inducible expression of a small set of recall genes that are critical for memory T cell function.

## Memory T cells exhibit distinct patterns of chromosome compartmentalization

Changes in 3D genome organization are intimately connected to gene regulatory dynamics and can facilitate or hamper transcriptional activation (*10*). Hence, we reasoned that 3D genome folding may provide memory T cells with an additional priming mechanism for efficient recall. For this, genome topology was profiled at high-resolution (5 kb; using ~1 billion valid interaction read pairs per condition) in resting and stimulated naive $CD4^+$ and memory $T_H2$ cells using in situ Hi-C with excellent overall reproducibility (fig. S5A; see data file S2 for dataset statistics).

We next assigned negative scores to B compartment and positive scores to A compartment genomic regions at 10- to 100-kb resolution [compartment scores (C-scores); Fig. 4A]. Although separated A and B compartments were detected in all conditions (fig. S5B), the overall compartmentalization strength was reduced specifically in resting memory $T_H2$ cells, which was normalized upon stimulation (Fig. 4B and fig. S5, B and C). PCA showed that C-scores were highly reproducible between replicates and readily distinguished naive $CD4^+$ from memory $T_H2$ cells, both before and after stimulation (Fig. 4C). Quantitative analysis of C-score dynamics at 10-kb resolution revealed compartmental repositioning of 21.1% of the genome ($\Delta$C-score > 0.3) across experimental groups, with a small fraction (0.13% of the genome) demonstrating very large changes ($\Delta$C-score > 1.0) (Fig. 4D). Although stimulation had the largest effects, nearly 9000 10-kb regions showed altered compartmentalization between resting naive and memory $T_H2$ cells (Fig. 4D). Most differences between naive $CD4^+$ and memory $T_H2$ cells involved C-scores increasing within the B compartment (i.e., BB to B), in line with decompaction of highly repressed chromatin (Fig. 4E and fig. S5D) (*49*). In contrast, stimulation predominantly triggered increased C-scores within the transcriptionally permissive A compartment in both naive and memory T cells (Fig. 4E and fig. S5D). These results show that resting memory T cells have distinct genome compartmentalization compared with naive cells, including a weaker separation of A and B compartments and a specific decompaction of heterochromatic regions.

We next focused on recall-associated changes in chromosome compartmentalization. Clustering analysis identified six groups of genomic regions ($n = 6888$ bins) that showed elevated C-scores upon stimulation and were already increased in resting memory $T_H2$ cells but not in resting naive T cells (Fig. 4F). Removal of singletons and stitching together consecutive bins (see Methods) yielded 754 regions of primed nuclear repositioning toward or more firmly within the A compartment (Fig. 4F). These regions were highly enriched for recall-associated open chromatin, $T_H2$ memory–specific superenhancers, GATA3 binding sites, and key inflammatory genes ($P < 1 \times 10^{-6}$, Fisher's exact test) (Fig. 4, F and G, and data file S3).

We observed strong spatial colocalization of recall-associated ATAC-Seq peaks at the level of compartmentalization (interactions within a 2- to 10-Mb window)—a feature specific to memory $T_H2$ cells and to memory-associated accessible chromatin sites (Fig. 4H and fig. S5E). Visualizing C-score dynamics at recall-associated open chromatin confirmed priming at both 1D (chromatin accessibility) and 3D (compartmentalization) levels (Fig. 4I). Regulatory elements linked to ($T_H2$-specific) recall genes showed stronger A-compartment membership in resting memory $T_H2$ cells (Fig. 4J and fig. S5F). This was particularly notable at the *MAF* locus, which contains 30.5% of all $\Delta$C-score > 1.0 bins. Here, combined 1D/3D chromatin priming in resting memory $T_H2$ cells is likely to underlie rapid transcriptional recall of *MAF* upon activation (Fig. 4K), which subsequently allows MAF to induce inflammatory gene expression (i.e., Fig. 3I). Conversely, stimulation-repressed inverse recall gene promoters exhibited weaker A compartment membership in both resting and activated memory $T_H2$ cells as compared with their naive counterparts (fig. S2E). Thus, priming of key recall genes in resting memory T cells is associated with spatial colocalization of these genes and their enhancers inside transcriptionally permissive nuclear compartments.

## Topological domain and loop reorganization associated with memory T cell function

Base-pair resolution analysis of 3D genome architecture revealed that most gene regulatory interactions occur within TADs (*50*). Insulation by TAD borders can potentially modulate transcriptional control in the context of memory T cell recall, e.g., by restricting or facilitating promoter-enhancer communication. We determined genome-wide insulation scores (see Methods) and identified 3647 reproducible TAD borders, of which 2184 (60%) were common to all four groups (Fig. 5, A and B). PCA using insulation score values at TAD borders readily and reproducibly distinguished resting from activated T cells (PC1) and naive from memory $T_H2$ cells (PC2)—even when only common borders were used (Fig. 5C). Thus, memory $T_H2$ cells exhibit unique global spatial genome insulation compared with naive cells already in a resting state, which is dynamically altered upon activation.

Most dynamic borders were associated with activation status, although others were only detected in specific cell types or states (fig. S6A). Quantitative clustering of insulation score patterns revealed that 70% of all TAD borders showed general activation–related dynamics, whereas 26% exhibited a pattern associated with a memory phenotype or recall-associated priming in resting memory $T_H2$ cells (Fig. 5, D and E, and fig. S6B). Most prevalent among the latter
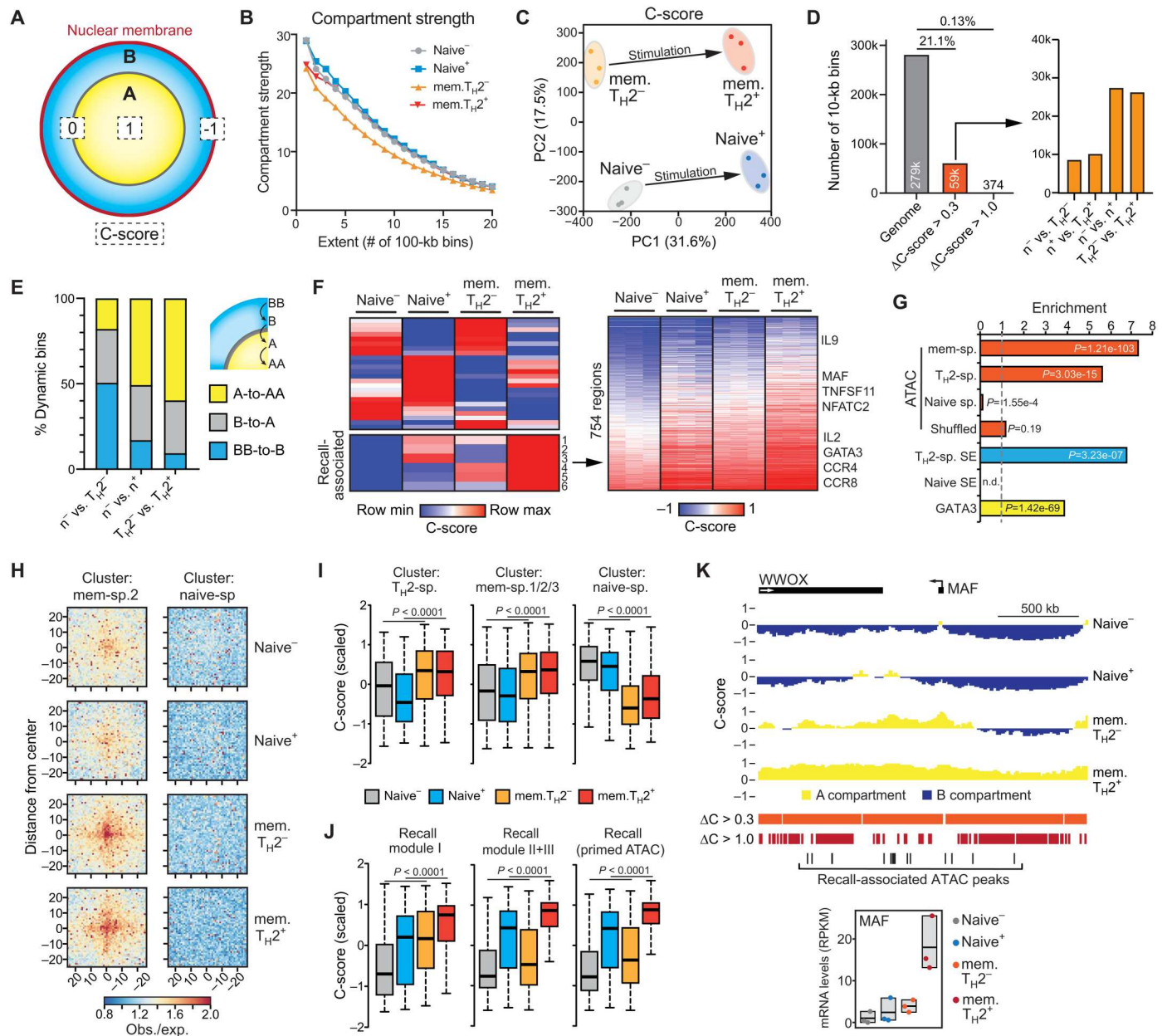
**Fig. 4. Distinct patterns of chromosome compartmentalization in human memory $T_H2$ cells are linked to transcriptional priming.** (**A**) Schematic representation of nuclear compartments A and B, including the C-score distribution used to quantify compartment association of genomic regions (i.e., from −1 = strong B to 1 = strong A). (**B**) Compartment strength calculated as a ratio between homotypic (AA/BB) and heterotypic (AB/BA) interactions over increasing distances. (**C**) PCA of genome-wide C-score values (10-kb bins). (**D**) Quantification of dynamic C-score bins (10-kb resolution) showing a 0.3 or greater difference in at least one comparison (n, naive CD4+ T cells; −, resting; +, stimulated). Assignment of dynamic bins to individual comparisons is indicated in the right bar graph. (**E**) Directionality of C-score changes across dynamic bins within the indicated comparisons. (**F**) Heatmap representation of clustered scaled C-scores (left). The six clusters showing a recall-associated increase in C-score consist of 754 regions further detailed in the right heatmap (with absolute C-score values), including examples of associated key inflammatory genes. (**G**) Enrichment scores and *P* values (Fisher's exact test) of recall-associated ATAC-Seq peaks (see Fig. 2 for definitions), $T_H2$-specific or naive-specific SEs, and GATA3 binding sites in memory $T_H2$ cells within the 754 dynamic C-score regions. (**H**) Meta-plot of long-range Hi-C interactions (2- to 10-Mb window) between recall-associated (cluster mem-sp.2) or naive-specific ATAC-Seq peaks. (**I**) Scaled C-scores (*z* score) of dynamic bins (ΔC-score > 0.1 in at least one pairwise comparison) at $T_H2$-specific (*n* = 220 bins), memory-specific (*n* = 1285 bins), and naive-specific (*n* = 414 bins) ATAC-Seq peak clusters. (**J**) Scaled C-scores (*z*-score) of dynamic bins at gene regulatory elements linked to recall-associated genes from recall module I (*n* = 654), the combined recall modules II + III (*n* = 2352; see Fig. 1F), and primed genes with an expression advantage ("primed ATAC," *n* = 897; see Fig. 2G). *P* values: Kruskal-Wallis test corrected for multiple testing. (**K**) Genome browser screenshot (top) showing C-score dynamics at the *MAF* locus, with gene expression dynamics depicted below boxplots.
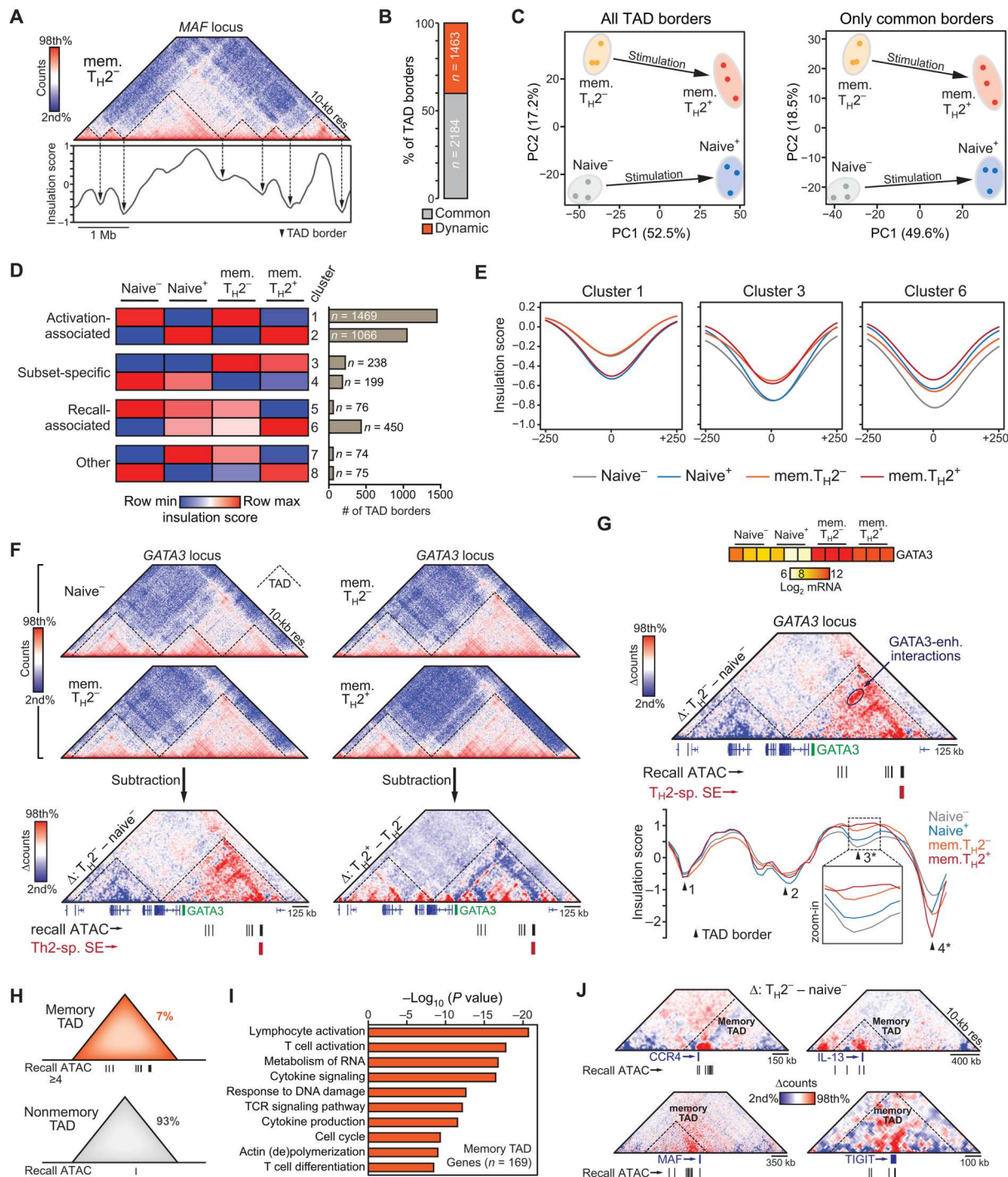
**Fig. 5. TAD dynamics linked to human memory T$_H$2 cell function.** (**A**) Hi-C interaction map of the *MAF* locus with insulation scores and TAD borders (defined as local minima) plotted below. (**B**) Proportions of common (invariant in all four sample groups) and dynamic (gained or lost in at least one sample group) TAD borders. (**C**) PCA of insulation score values at all (left) or only common (right) TAD borders. (**D**) Heatmap representation of clustered scaled insulation scores at TAD borders. Patterns associated with clusters are indicated on the left; border counts for each cluster are shown on the right (bar graph). (**E**) Average insulation scores at dynamic TAD borders from the indicated clusters in resting (−) or stimulated (+) naive CD4$^+$ T cells and memory T$_H$2 cells. (**F**) Hi-C interaction maps of the *GATA3* locus from the indicated sample groups. Signal subtraction (delta) plots are shown below to highlight differences in interaction signals (left: red = higher in T$_H$2$^-$ versus naive$^-$; right: red = higher in T$_H$2$^+$ versus T$_H$2$^-$). Locations of genes, recall-associated ATAC-Seq peaks, and T$_H$2-specific SEs are indicated at the bottom. (**G**) Top: heatmap depicting *GATA3* mRNA levels. Middle/bottom: Hi-C signal subtraction plot (red = higher in T$_H$2$^-$ versus naive$^-$) as shown in (F) (left side) but with insulation score profiles and TAD border calls (*n* = 4) indicated below. Note the third dynamic TAD border that is only called in naive T cells. (**H**) Definition of "memory TADs" as those domains that contain four or more recall-associated ATAC-Seq peaks (7% of all TADs). (**I**) Pathway enrichment analysis of recall-associated genes located within memory TADs. (**J**) Hi-C signal subtraction plots (red = higher in T$_H$$^-$ versus naive$^-$) for selected memory TADs.

category are borders ($n$ = 450) that are already weakened in resting memory $T_H2$ cells before further loss of insulation score upon activation. A prime example hereof is the *GATA3* locus, which is located within a large and highly dynamic TAD (Fig. 5F). The *GATA3* TAD contains a weaker internal border in naive cells that is dissolved in memory $T_H2$ cells, allowing for robust interaction of *GATA3* with downstream regulatory regions (including a $T_H2$-specific superenhancer) and transcriptional up-regulation (Fig. 5, F and G). Stimulation focuses *GATA3*-enhancer interactions and strengthens the downstream TAD border (Fig. 5, F and G), possibly to increase *GATA3* transcriptional robustness.

Specific clusters of dynamic borders showed enrichment or depletion for recall-associated accessible chromatin sites (fig. S6C). We noticed that a small number of TADs ($n$ = 256; 7% of total) harbor ~50% of all recall-associated ATAC-Seq peaks (Fig. 5H). Genes within these "memory TADs" are involved in T cell activation, including many genes from the three recall-associated transcriptional modules ($n$ = 169 of 884; $P$ = 0.0001, Fisher's exact test) (Fig. 5I and data file S3). In addition, memory TADs were strongly enriched for dynamic C-score bins (enrichment ratio: 13.1; $P$ < 0.0001, Fisher's exact test). Increased intradomain interactions were already present in many memory TADs in resting memory $T_H2$ cells, revealing increased topological chromatin connectivity around key recall genes and nearby regulatory elements—irrespective of their activation status (i.e., the active *CCR4* or inactive *IL13* gene) (Fig. 5J and fig. S6D).

Gene regulatory elements can interact via focused 3D interactions often referred to as chromatin loops. Loop detection using Mustache (*51*) identified thousands of strong interaction foci in each condition (fig. S7A). We first focused on activation-associated loops already present in resting memory $T_H2$ cells as optimal candidates for priming for transcriptional recall, identifying hundreds of loops specifically associated with a memory phenotype and/or recall (Fig. 6A and fig. S7B). Anchor regions of these memory-associated loops were strongly enriched for regulatory elements, with >75% forming interactions between promoters and/or enhancers (Fig. 6B and fig. S7C). This is illustrated by the *GATA3* memory TAD in which memory-specific loops connect *GATA3* to primed (super)enhancers (Fig. 6C). Genes linked to memory-associated loops encoded regulators of cell adhesion, T cell activation, and the cell cycle, which showed a significant transcriptional activation advantage specifically upon memory recall (Fig. 6, D and E, and data file S3). Similar results were obtained when using a broader definition of memory-associated loops (i.e., including the 2198 and 3675 $T_H2$-specific loops) (fig. S7D). Regulatory connections involving these genes were formed in resting memory $T_H2$ cells without significant gene induction. This is exemplified by the *IL9* locus, in which two memory-specific loops create an interaction domain in which *IL9* is connected to downstream recall-associated regulatory elements (Fig. 6F). Upon activation, only memory $T_H2$ cells rapidly and markedly up-regulate *IL9* expression (Fig. 6G).

We next examined loop sets unique to naive T cells. We reasoned that the absence of such loops in memory $T_H2$ cells may be linked to recall-associated transcriptional silencing or—in the case of repressive loops—facilitating transcriptional recall upon stimulation. Loops present only in naive cells irrespective of stimulation status ($n$ = 514) were enriched for enhancer interactions (fig. S7E). Genes associated with these loops were down-regulated upon naive $T_H$ cell stimulation and already repressed in resting memory $T_H2$ cells—

akin to an "inverse recall" pattern (fig. S7E). In contrast, loops only detected in resting naive cells ($n$ = 3850) were highly enriched for promoter-promoter interactions. Unexpectedly, genes linked to these loops were up-regulated upon TCR stimulation in memory $T_H2$ cells and enriched for general biological processes associated with cellular activation (fig. S7F). These findings indicate the existence of repressive loops connecting promoters of activation-inducible genes in naive cells, which are already decommissioned in resting memory $T_H2$ cells.

The signature $T_H2$ cytokine genes *IL4-IL5-IL13* are organized as a cluster and exclusively up-regulated upon memory $T_H2$ cell activation (see Fig. 1D). Studies in murine $T_H2$ cells have identified several distal enhancers organized in a locus control region (LCR) that control cytokine gene expression through long-range interactions (*52*), although 3D folding of the human $T_H2$ cytokine locus and the relationship with memory recall remain unexplored. We observed robust yet nonpunctate 3D interactions across the entire $T_H2$ locus already in resting naive $T_H$ cells, which were more abundant in memory $T_H2$ cells and further augmented upon memory cell activation (Fig. 6H and fig. S7G). High-resolution analysis (5 kb) showed significantly increased nuclear proximity of *IL5*, *IL4*, *IL13*, and the LCR in resting memory $T_H2$ cells as compared with naive cells (Fig. 6, I and J). These findings are consistent with priming of inflammatory genes for efficient recall through altered local 3D genome organization, i.e., by maintaining elevated promoter-enhancer interaction frequencies in the absence of activating signals. The *IL9* and $T_H2$ cytokine loci were primed at both 1D (i.e., chromatin accessibility) and 3D (i.e., promoter-enhancer contacts) epigenomic levels. We observed widespread multiscale priming within the core T cell activation–associated recall program (Fig. 6K and fig. S7H), including all major inflammatory cytokine genes and the *CD28-ICOS-CTLA4*, *CCR4*, and *MAF* loci (fig. S8 and data file S1). $T_H2$-specific recall genes were particularly enriched for priming at the 3D level (i.e., 100% of primed genes) (fig. S7H). TF motif enrichment analyses on accessible chromatin sites within regions of recall-associated 3D genome reorganization implicated AP-1, RUNX, ETS, and IRF family proteins as well as CTCF in priming genome conformation in resting memory cells (fig. S7I).

In summary, resting memory T cells uphold a uniquely modified topological domain and loop organization. This 3D genome conformation poises genes for rapid transcriptional recall by increasing the spatial proximity between memory recall genes and their primed regulatory elements or through the loss of repressive promoter-promoter interactions.

## Multiscale epigenomic priming in memory T cells is linked to asthma

We next investigated whether the recall-associated transcriptional and epigenomic signatures we identified could be linked to memory T cell dysfunction in human disease. Asthma is one of the most common chronic inflammatory disorders, with most patients exhibiting excessive pulmonary type 2 inflammation often driven by aberrant memory $T_H2$ cell activity (*6*, *7*). We performed RNA-Seq on resting memory $T_H2$ cells from peripheral blood samples of healthy controls and patients with asthma with either mild-to-moderate or severe disease (i.e., low or high symptom burden; see Methods and table S1). We observed increased expression levels of all three recall gene modules in memory $T_H2$ cells from patients with asthma compared with healthy controls (Fig. 7A and
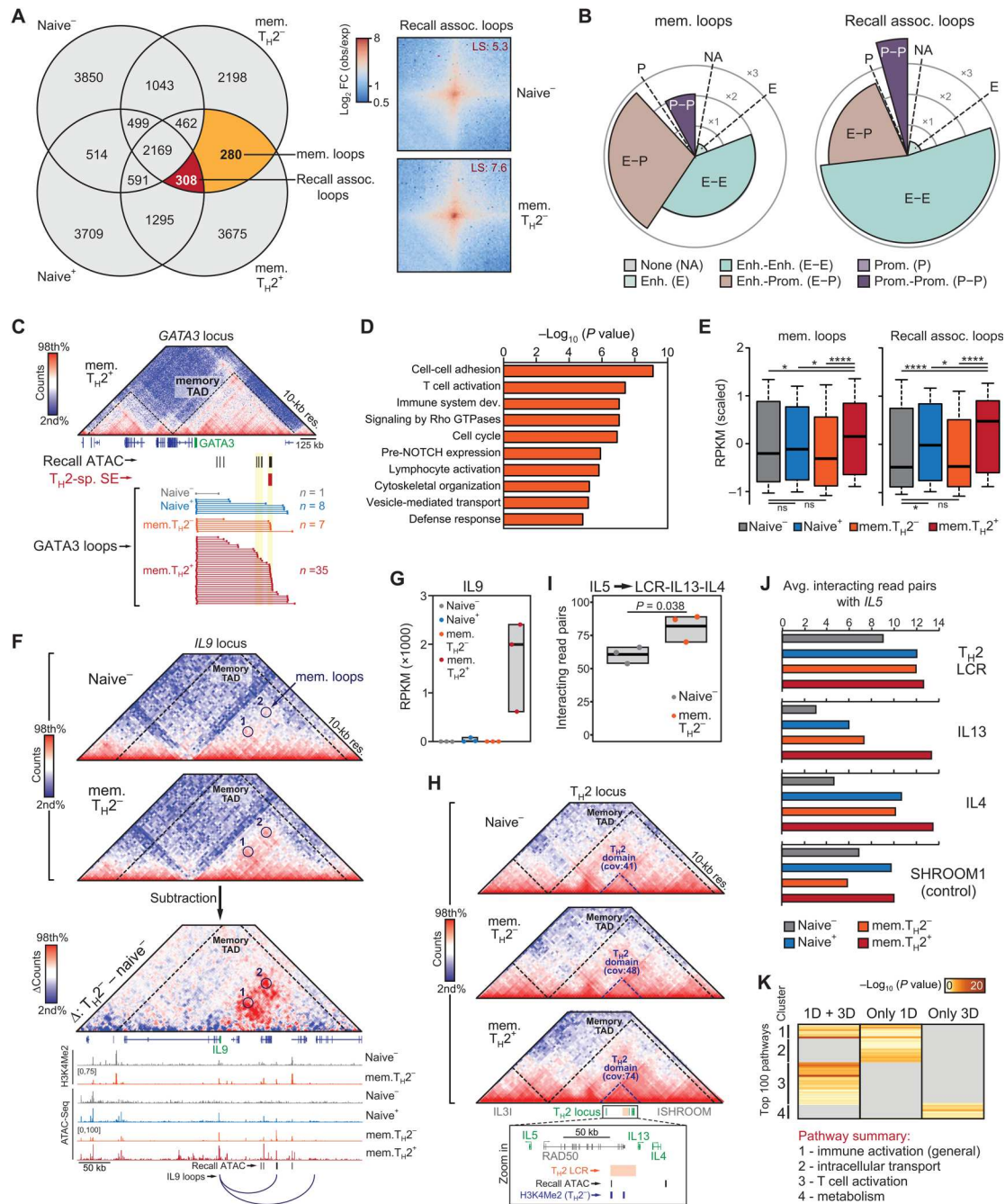
**Fig. 6. Chromatin loops prime genes for rapid recall in human memory T$_H$2 cells.** (**A**) Venn diagram of all loops identified in resting (−) or stimulated (+) naive CD4$^+$ T cells and memory T$_H$2 cells. Meta-plots of Hi-C signal intensity averaged across all recall-associated loops ($n = 308$) in resting naive and memory T cell subsets are shown on the right. LS, loop strength (log$_2$ scale). (**B**) Combined pie chart and radar plot depicting the proportion of memory and recall-associated loops connecting enhancers (Enh./E) and/or promoters (Prom./P). The height of each pie segment indicates fold enrichment (denoted by the gray circles). (**C**) Hi-C interaction maps of the *GATA3* locus in stimulated memory T$_H$2 cells. Locations of genes, recall-associated ATAC-Seq peaks, and T$_H$2-specific SEs are indicated below, followed by significant loops involving the *GATA3* promoter detected in each condition. (**D**) Pathway enrichment analysis of genes ($n = 838$) near anchors of memory and recall-associated loops. (**E**) Scaled mRNA expression (z-score) of genes near anchors of memory (left, $n = 430$) or recall-associated (right, $n = 425$) loops in resting (−) or stimulated (+) naive CD4$^+$ T cells and memory T$_H$2 cells. $P$ values: Kruskal-Wallis test corrected for multiple testing. (**F**) Hi-C interaction maps and signal subtraction plot (bottom; red = higher in T$_H$2$^-$ versus naive$^-$) of the *IL9* locus. H3K4Me2 ChIP-Seq and ATAC-Seq signal tracks are shown below as well as loops involving the *IL9* gene specifically detected in memory T$_H$2 cells. (**G**) *IL9* gene expression levels in the indicated sample types. (**H**) Hi-C interaction maps of the T$_H$2 cytokine locus. Locations of genes, the T$_H$2 LCR, recall-associated ATAC-Seq peaks, and H3K4Me2 peaks are indicated below (zoom in). Median read count per 10-kb bin [coverage (cov)] within the T$_H$2 domain is indicated. (**I**) Interacting read pairs detected connecting *IL5* with the LCR-*IL13-IL4* region (sum of 5-kb bins) in resting naive or memory T cells. $P$ value: Mann-Whitney $U$ test. (**J**) Interacting read pairs detected connecting *IL5* with the T$_H$2 LCR, *IL13*, *IL4*, or the unrelated *SHROOM1* gene across the indicated sample types. (**K**) Heatmap showing pathway enrichment for the indicated primed recall gene sets. Pathway cluster ($n = 4$) functions are summarized below.

**Fig. 7. Multiscale epigenomic priming in human memory T_H2 cells is linked to asthma.** (**A**) Gene expression levels (z-score–scaled) of the three recall-associated transcriptional modules (see Fig. 1) as measured in peripheral blood memory T_H2 cells from healthy controls or patients with asthma with either low or high symptom burden. (**B**) mRNA levels of a primed recall gene (*MAF*) and a general activation marker (*CD40LG*) across the indicated groups. (**C**) H3K4Me2 levels (z-score–scaled) at the four recall-associated ATAC-Seq peak clusters as measured by ChIP-Seq on peripheral blood memory T_H2 cells from healthy controls or patients with asthma. (**D**) Genome browser screenshot of the *CD82* locus showing H3K4Me2 signals in a healthy control and a patient with asthma. Inset graph below shows H3K4Me2 levels at the indicated recall-associated ATAC-Seq peak across the entire cohort (HC, healthy; AST, asthma). (**E**) Enrichment scores and P values for asthma-associated SNPs intersected with recall-associated or naive-specific ATAC-Seq peaks. (**F**) Genome browser screenshot of the *CCR4-GLB1* locus, highlighting a T_H2-specific SE region containing multiple recall-associated ATAC-Seq peaks and asthma SNPs. (**G**) Enrichment scores and P values for asthma-associated SNPs intersected with the indicated recall-associated 3D genome features. (**H**) Graphical summary of this study's main findings. See text for details. Statistical tests used: (A and B) Kruskal-Wallis test corrected for multiple testing; (C and D) Mann-Whitney U test; (E and G) Fisher's exact test. **P < 0.01 and ****P < 0.0001.
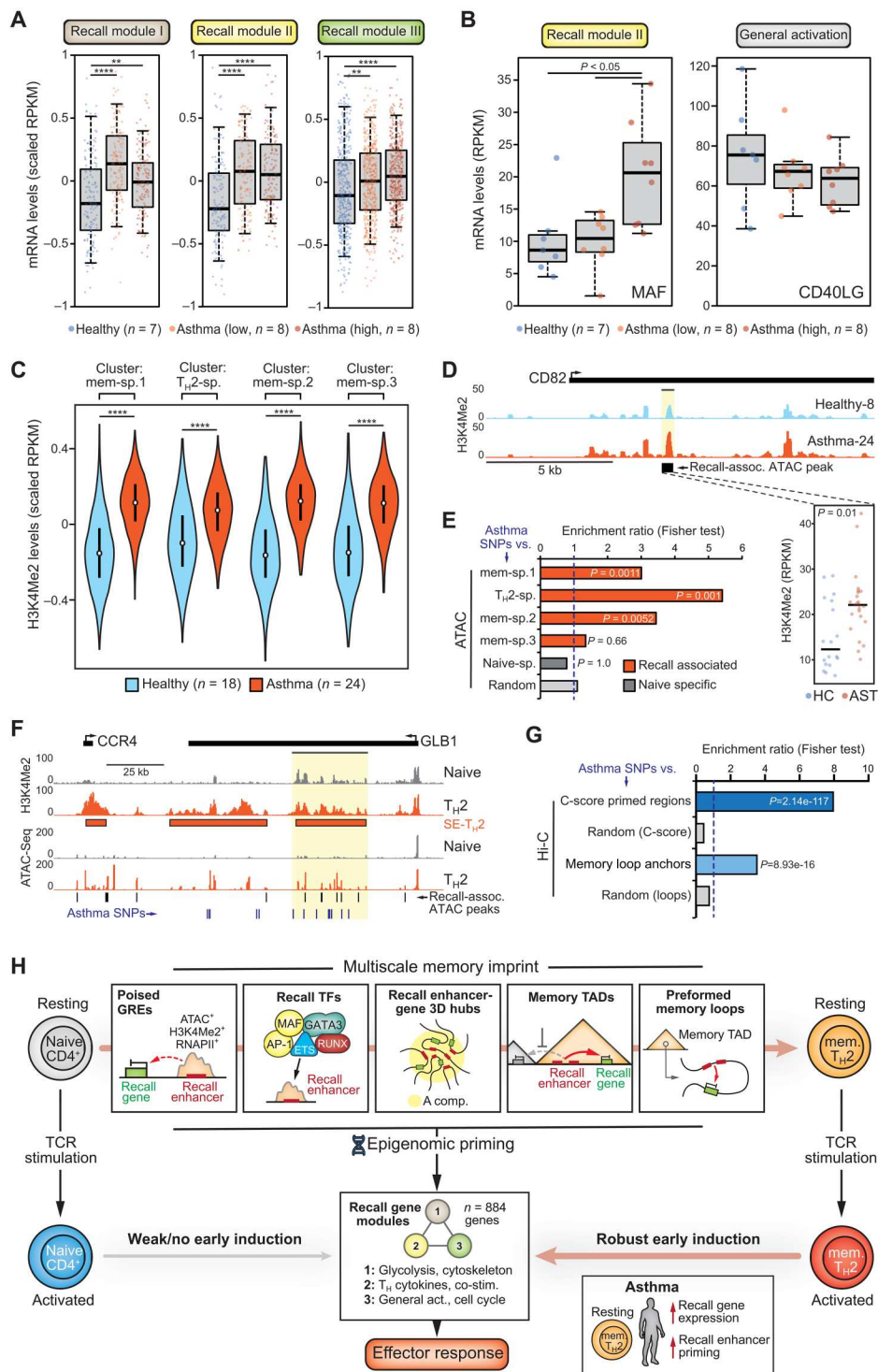
fig. S9A), which were less pronounced for general activation genes (fig. S9, A and B). For example, expression of the *MAF* recall gene was increased in patients with severe asthma, whereas the levels of general activation marker *CD40LG* were unaltered (Fig. 7B). In addition, analysis of published resting memory T_H2 cell H3K4Me2 profiles from patients with asthma (*53*) revealed consistently higher H3K4Me2 levels at recall-associated ATAC-Seq peak clusters

in asthmatics compared with healthy controls, e.g., at the primed *CD82* locus (Fig. 7, C and D). In contrast, only marginal differences were observed at naive-specific accessible chromatin sites (fig. S9, C and D). Together, these findings demonstrate increased activity of the primed molecular circuits that promote rapid recall in resting disease-associated memory T_H2 cells.

We then intersected the location of single-nucleotide polymorphisms (SNPs) linked to asthma pathophysiology (54) with the clusters of recall-associated regions of chromatin accessibility in memory CD4$^+$ T cells. Most memory-specific clusters showed statistically significant positive enrichment scores (in particular $T_H2$-specific peaks), which were not observed in randomly shuffled or in naive-specific peaks (Fig. 7E). $T_H2$-specific superenhancer regions were particularly enriched for asthma-associated SNPs (enrichment ratio: 31.79; $P < 0.0001$, Fisher's exact test), as illustrated by a primed superenhancer in the *CCR4-GLB1* locus in which asthma SNPs colocalized with recall-associated ATAC-Seq peaks (Fig. 7F). We detected a significant enrichment of asthma-associated variants within recall-associated and memory-specific changes in 3D genome organization (Fig. 7G), revealing links between the genetic susceptibility to asthma and epigenomic priming of memory $T_H2$ cells at both 1D and 3D levels.

## DISCUSSION

In this study, we show that in contrast to naive CD4$^+$ T cells, human memory $T_H$ cells maintain a distinct 1D/3D chromatin landscape that primes modules of selected recall genes for rapid transcriptional activation to facilitate near-instant immune effector responses. More specifically, our analyses indicate that efficient transcriptional recall of resting human memory $T_H2$ cells builds on several epigenomic hallmarks: (i) maintenance of transcriptionally permissive chromatin at stimulation-induced (super)enhancers; (ii) increased activity of a set of specific TFs at these recall enhancers, both at baseline and after activation; (iii) spatial compartmentalization of recall genes and enhancers in 3D chromatin hubs; (iv) increased connectivity of recall genes and enhancers within memory TADs; and (v) preformed chromatin loops connecting recall genes and their enhancers (Fig. 7H). In a quiescent memory $T_H2$ cell, these memory-specific epigenomic features position hundreds of genes in a spatial chromatin environment that is exceptionally conducive to rapid transcriptional reactivation. Efficient induction of recall genes, comprising ~3% of the transcriptome, allows memory $T_H$ cells to quickly adapt their metabolic, migratory, and inflammatory profile to launch specialized adaptive immune responses. Notably, we provide evidence that dysregulation of the molecular mechanisms controlling recall occurs in patients with chronic inflammatory disease.

Previous studies reported maintained active chromatin signatures in resting memory(-like) T cells at regulatory elements of inflammatory genes (27–29, 55–57). Our findings confirm and substantially extend these data by revealing that resting human memory CD4$^+$ cells carry an epigenomic imprint of TCR stimulation and lineage (e.g., $T_H2$) specification that consists of ~3000 genomic elements marked by accessible chromatin, H3K4Me2 deposition, and RNAPII recruitment. This epigenetic signature has previously been associated with short-term transcriptional memory in yeast, fruit fly, and human cells in response to hormones, nutrient deprivation, or cytokines (58, 59). Maintaining such a transcriptionally permissive chromatin environment at key regulatory elements controlling inflammatory gene expression—including 80% of memory-specific superenhancers in $T_H2$ cells—provides a mechanistic basis for rapid induction of recall module genes. Supporting this concept, murine memory $T_H2$ cells with reduced levels of the H3K4 methyltransferase KMT2A (also called MLL) failed to maintain H3K4Me2 levels at the $T_H2$ cytokine locus and showed impaired secondary responses in vivo (60).

Unexpectedly, we identified genome topology as the best global discriminator of naive and memory cell $T_H$ cell phenotypes (i.e., in a PCA)—in both resting and activated states. Compared with naive cells, resting memory $T_H2$ cells exhibit a less rigid A/B compartment separation, show hallmarks of heterochromatin decompaction, and carry ~700 genomic regions more strongly associated with transcriptionally permissive nuclear compartments. At this topological level, primed recall-associated (super)enhancers form 3D hubs by engaging in long-range interactions specifically in memory $T_H2$ cells. More locally, recall genes and their regulatory elements often reside in memory TADs, which compared with naive cells exhibit increased intra-TAD interaction frequencies connecting recall gene promoters to their enhancers before activation. An illustrative example of multiscale epigenomic priming is the *MAF* locus encoding an AP-1 family TF previously linked to the control of $T_H(2)$ cell fate and function (46, 61). In resting memory $T_H2$ cells, the poorly expressed *MAF* gene resides in a TAD that is already positioned in the A compartment. Recall-associated distal enhancers inside the *MAF* memory TAD are already accessible and engage in interactions with *MAF* before stimulation. Hence, a specific 1D-3D chromatin organization readily explains the rapid and specific induction of *MAF* in memory $T_H2$ cells upon TCR activation.

The mechanisms that maintain and exploit the primed epigenomic landscape of human memory T cells have remained elusive. Our analyses converge on AP-1 TFs—known to act downstream of TCR signaling (62)—and lineage-determining TFs such as GATA and RUNX proteins as key regulators of rapid recall in human CD4$^+$ T cells. We find that primed recall enhancers are strongly enriched for motifs of these TFs, of which several are already expressed in memory T cells before TCR stimulation (see Fig. 3). After TCR stimulation, AP-1 TFs and GATA3 occupy most of the recall-associated regulatory regions. Chemical inhibition of AP-1 TF activity or preventing MAF induction in memory $T_H2$ cells selectively blunted the transcriptional induction of several recall genes, partially decoupling the reactivation of memory-linked genes from the general T cell activation program—at least at the time scales chosen here (i.e., 24 hours). On the basis of these findings, we propose a model in which signal-responsive AP-1 TFs (e.g., BATF and FOSL2) cooperate with lineage-specifying TFs (e.g., GATA and RUNX proteins) to maintain a 1D/3D primed epigenome in quiescent human memory T cells, akin to the recently described role of TCF-1 in epigenomic priming of murine CD8$^+$ memory T cells (63). Upon TCR stimulation, these "recall TFs" can immediately initiate transcriptional (re)activation of the three recall gene modules, which boosts their own expression and de novo activates other TFs (e.g., MAF) to maximize transcriptional output of the ~900 recall genes. These findings are in line with studies performed in murine memory(-like) T cells, which have reported JUND, ETS1, and RUNX1 binding to sites that remained accessible after a previous episode of stimulation (29, 64, 65).

At the 3D level, we envision two broad mechanisms through which recall TFs may install primed genome topology: first, through modulating chromatin loop extrusion by CTCF and cohesin, which is critical for the formation of TAD borders and a subset of gene regulatory interactions (11, 12, 14). For example, the AP-1 factor BATF was shown to cooperate with CTCF to organize

promoter-enhancer interactions at cytokine loci in murine $T_H17$ cells (66), and the lineage-determining TF TCF-1 was recently implicated in recruiting cohesin (67) or CTCF (41, 63) to active enhancers in naive T cells and their thymic precursors. Moreover, macrophages deficient in CTCF (68) or cohesin (69) showed impaired activation of inducible genes upon stimulation. Second, multivalent interactions between TFs and their cofactors may promote nuclear compartmentalization of regulatory regions through condensate formation (70). Our observation of 3D recall enhancer hubs forming at megabase scales in human memory $T_H2$ cells reveals nuclear compartmentalization of recall-associated genomic elements and regulatory proteins. Concentrating (super)enhancers, key TFs, and transcriptional machinery in the vicinity of genes targeted for recall already in a resting state, possibly through condensate formation, could greatly facilitate rapid transcriptional activation of the compartmentalized genes by recall TFs upon TCR activation. Important to note is that our results do not establish a direct causal link between genome conformation and enhanced transcriptional induction of recall genes in human memory $T_H$ cells. For this, additional experiments aimed at precise disruption of local 3D genome folding (e.g., using genome editing) are required.

A remaining open question is how the primed 1D/3D chromatin landscape of human memory T cells is maintained across multiple cell divisions and over extended periods of time [e.g., >10 years (71)]. At the 1D level, recall TFs may be actively involved in the maintenance of accessible chromatin or the H3K4Me2 mark on primed recall enhancers, e.g., by recruiting chromatin-modifying enzymes. GATA3 was previously shown to activate transcription in a complex with KMT2A/MLL in human $T_H2$ cells (72), and AP-1 factor activity is important for establishing accessible chromatin during human T cell activation (44)—presumably via recruiting SWI/SNF chromatin remodeling complexes (73). The IL-2–inducible AP-1 factor JUND appeared to support the maintenance of chromatin accessibility at enhancers activated by stimulation in a murine in vitro model system of T cell priming (29, 65).

IL-7 and IL-15 signaling, both resulting in signal transducer and activator of transcription 5 (STAT5) TF activation, are critical for homeostasis of resting memory T cells (74). Previous work has implicated the IL-7/STAT5 axis in maintaining chromatin accessibility at a subset of primed regulatory elements in murine memory-like CD4$^+$ T cells (65), although our analyses did not detect STAT motifs enriched in the recall enhancer landscape of human memory CD4$^+$ T cells. Nevertheless, it remains possible that STAT5 controls a small subset of primed enhancers or acts in TF complexes without binding the DNA itself. It should be noted that alternative mechanisms of priming memory T cells—not necessarily only acting at the chromatin level—have been described and are likely to function in concert with TF-mediated epigenomic priming to enable rapid recall. For example, immediate translocation of nuclear factor κB (NFκB) proteins from the cytoplasm into the nucleus was shown to underlie the more rapid activation of *Ifng* in murine memory CD4$^+$ T cells as compared with naive cells (75). We also detected NFκB recruitment to a small subset (~6%) of recall enhancers after TCR activation (see Fig. 3F). Release of the translation repression of preformed mRNAs has also been implicated in rapid recall (76), as well as metabolic reprogramming and altered TCR signal transduction (77, 78).

Last, our analyses show that recall-associated gene modules and their primed regulatory elements exhibit increased biochemical activity in resting memory $T_H2$ cells from patients with asthma, who suffer from chronic pulmonary type 2 inflammation. Furthermore, we found that genetic variants linked to asthma pathophysiology are enriched in recall enhancers. These findings suggest that circulating quiescent memory $T_H2$ cells in patients with asthma may reside in a cell-intrinsic "hyperprimed" state—possibly shaped by genetics—that lowers the threshold for recall and fuels the accumulation of activated pathogenic memory $T_H2$ cells in the lungs. Future studies are required to validate this concept, which may offer new opportunities for therapy development and could be extended to other contexts of memory T cell dysfunction such as autoimmunity or cancer.

## MATERIALS AND METHODS
### Study design
Human naive and $T_H2$ memory CD4$^+$ T cells were isolated from healthy donor blood in resting (ex vivo) and activated (in vitro) states. To identify transcriptional and epigenomic signatures that predispose memory T cells to a more efficient transcriptional induction of the associated genes upon activation (i.e., recall), we used transcriptomic (RNA-Seq; $n = 3$ independent biological replicates), 1D epigenomic (ATAC-Seq; $n = 3$ or 4 independent biological replicates), and 3D epigenomic (Hi-C; $n = 3$ independent biological replicates) data. Recall-associated transcriptional and epigenomic signatures were confirmed using flow cytometry ($n = 2$ or 3 independent biological replicates) and CRISPR-Cas9 genome editing ($n = 2$ or 3 independent biological replicates) and by integrating published epigenomic datasets. Last, we generated bulk transcriptome data of peripheral blood memory $T_H2$ cells obtained from patients with asthma ($n = 16$) and healthy donors ($n = 7$), which we integrated with public H3K4me2 ChIP-Seq data and linked to known asthma-associated genetic variants.

### Human T cell isolation from healthy donors and patients with asthma
Primary sources of T cells from healthy individuals in this study were buffy coats (from 500 ml of peripheral blood samples) obtained from the Sanquin Bloodbank (Amsterdam, Netherlands). Informed consent was obtained by Sanquin. For asthma patient materials used in this study, criteria for diagnosis, inclusion, and classification (79) are outlined in the Supplementary Materials and table S1. Peripheral blood mononuclear cells (PBMCs) were isolated as previously described (80). From PBMCs, CD4$^+$ T cells were isolated using the human CD4$^+$ T Cell Isolation Kit (Miltenyi Biotec) according to the manufacturer's instructions, followed by FACS (using FACSAria II, BD Biosciences) to isolate resting naive CD4$^+$ T cells (live single CD4$^+$CD127$^+$CD25$^{neg}$CD45RA$^+$ cells) and $T_H2$ cells (live single CD4$^+$CD127$^+$CD25$^{neg}$CD45RA$^{neg}$CCR6$^{neg}$-CXCR3$^{neg}$CXCR5$^{neg}$CCR4$^+$ cells). Antibodies used for FACS are listed in table S2. Fluorescent antibody staining methods are in the Supplementary Materials.

### In vitro T cell activation
Freshly isolated T cells were activated in vitro at $1 \times 10^6$ cells per ml in T cell culture medium [RPMI 1640 (Gibco), 10% fetal calf serum (HyClone), 55 μM 2-mercaptoethanol (Sigma-Aldrich), 2 mM L-

alanyl-L-glutamine (GlutaMAX, Gibco), 1 mM sodium pyruvate (Gibco), 0.1 mM nonessential amino acids (Gibco), penicillin/streptomycin (Gibco), 10 mM Hepes (Gibco), and recombinant human IL-2 (50 U/ml; R&D Systems)] in round-bottom 96-well culture plates using Human T-Activator CD3/CD28 Dynabeads (Thermo Fisher Scientific) in a 1:1 bead-to-cell ratio at 37°C, 5% $CO_2$ for 24 hours. Activator beads were not removed before further processing of samples to minimize loss of activated cells.

### RNA isolation, qPCR, and RNA-Seq
RNA was extracted from ~50,000 resting cells per condition using an RNeasy Micro kit (Qiagen) according to the manufacturer's instructions. For quantitative polymerase chain reaction (qPCR), RNA was synthesized into complementary DNA using RevertAid H Minus Reverse Transcriptase and random hexamer primers in the presence of RiboLock RNAse inhibitor (Thermo Fisher Scientific). qPCR was performed using 7.5 μl of 2× SYBR Green Universal Master Mix (Life Technologies) and 6 pmol of both forward and reverse primers, added to a total reaction volume of 15 ul using nuclease-free water. Primer sequences used can be found in table S3. For high-throughput sequencing of RNA, libraries were prepared using Smart-seq2 methodology (81) and sequenced according to the Illumina TruSeq Rapid v2 protocol on an Illumina HiSeq2500 [single read, 51–base pair (bp) read length].

### CRISPR-Cas9 genome editing and AP-1 TF perturbation
For genome editing in primary human memory $T_H2$ cells, we adopted the method published by Seki and Rutz (82), which we describe in more detail in the Supplementary Materials. Crispr RNAs (crRNAs) specific for *MAF* were designed using Benchling software (see table S3 for crRNA sequences). AP-1 factor inhibition experiments are described in the Supplementary Materials.

### RNA-Seq data processing and differential gene expression analysis
Reads were aligned to the hg38 build of the human reference genome using HISAT2 (83). Raw counts and RPKMs were determined on the exons of RefSeq-annotated genes using HOMER's [v4.11 (84)] analyzeRepeats.pl command. Differentially expressed genes [false discovery rate (FDR) < 0.1] were identified using DESeq2 (85) through HOMER's getDiffExpression.pl command. In all downstream analyses, we only included genes that were expressed in at least one relevant group (RPKM > 1 in ≥50% of replicates). PCA was conducted using FactoMineR (86). *K*-means clustering was performed using PAST (87). Heatmaps, including hierarchical clustering on gene expression values, were generated using Morpheus (https://software.broadinstitute.org/morpheus/). Pathway enrichment analysis on differentially expressed genes and summarizing enriched pathways into gene-based networks were performed using Metascape (88).

### Identification of recall-associated and general activation transcriptional signatures
The strategies used to define the various recall-associated and general activation transcriptional signatures identified in this study are detailed in the Supplementary Materials.

### ATAC-Seq data processing, peak calling, and assignment of peaks to genes
ATAC-Seq data were previously published by Calderon *et al.* (15) (GSE118189). SRA files were aligned to hg38 with HISAT2. Insert sizes >500 bases were removed using SAMtools (89). Tag directories were created using HOMER's makeTagDirectory command, after which reads aligning to the Y chromosome or mitochondrial DNA were removed, and the fragment length estimate was set to 77 as a representative estimate for all samples. A transcription start site (TSS) enrichment ratio was calculated using HOMER's annotatePeaks.pl command (tss hg38 -size 10000 -hist 40) as the average TSS signal (−80 to +80 bp from TSS), divided by the average local background signal (−5 to −4.92 kb and +4.92 to +5 kb from TSS), to use as a measure for relative sample quality. Samples with a TSS enrichment ratio less than the mean-SD TSS enrichment ratio across all samples were excluded from further analysis. Peak calling was performed using HOMER's findPeaks command (-region -size 100 -minDist 75). Reproducible peaks per experimental group were defined as overlapping peaks called in three of three replicates (three of four for activated memory $T_H1$ and activated naive CD4+ T cells) using HOMER's mergePeaks command. Universal peaks were similarly identified as overlapping reproducible peaks found in all eight experimental groups using mergePeaks. HOMER was used to create bedgraph files for visualization in the IGV genome browser (90). Peaks were associated with genes using GREAT (91) with default settings (i.e., basal plus extension; proximal: 5 kb upstream, 1 kb downstream, distal: up to 1000 kb). When more than two genes were linked to a single peak, only the closest two genes were included in downstream analyses.

### ATAC-Seq peak signal normalization and differential analysis
Raw counts were determined at all reproducible peaks found in at least one of eight experimental groups using HOMER's annotatePeaks.pl command (hg38 -size given -raw). Raw counts were rounded down to the nearest integer. Counts at peaks were normalized by slightly adapting the standard normalization method of DESeq2. Scaling factors were determined for each sample based on the set of universal peaks with DESeq2. Next, those scaling factors were used to normalize counts at all peaks. This adaptation of DESeq2's established normalization method allowed us to successfully normalize ATAC peak counts despite the approximately doubled number of ATAC-Seq peaks upon T cell activation and the relative lack of zeros in ATAC-Seq data (compared with RNA-Seq) at regions where there is no true signal. PCA was conducted using FactoMineR. Differentially enriched ATAC-Seq peaks were identified using DESeq2 ($log_2$ fold change > 1, FDR < 0.05). Clustering was performed on differentially accessible sites across all cell states ($n = 32,847$ peaks) using Mfuzz (92). Clusters were selected on the basis of visual inspection of patterns; high-confidence peaks ($\alpha > 0.5$) were kept for downstream analyses and visualization. Histograms of the ChIP-Seq signal were generated using HOMER's annotatePeaks. Heatmaps were generated using Morpheus, and pathway enrichment analysis on associated genes was performed using Metascape.

### TF binding motif identification
HOMER's findMotifsGenome command (-size 200 -mask) was used to search for overrepresented TF binding motifs in genomic

regions. The top three ranked de novo motifs based on $P$ value were selected for further analysis.

### ChIP, ChIP-Seq, and data analysis

H3K4Me2 ChIP-Seq data were generated using the ChIPmentation protocol as previously described (39, 47). More details can be found in the Supplementary Materials. Reads were aligned to the hg38 build of the human reference genome using HISAT2. H3K4Me2-enriched regions were identified using HOMER's findPeaks command (-region -size 1000 -minDist 2500); for superenhancers, the parameters -style super -L 1 were used instead with a negative control mock (rabbit immunoglobulin G) experiment as background. H3K4Me2 signals were quantified at recall-associated ATAC-Seq peaks or peak clusters using HOMER's annotatePeaks.pl command. BEDTools' (93) fisher command was used to calculate the overlap between genomic features. Similar methodology was used to analyze publicly available ChIP-Seq datasets.

### Asthma-associated SNPs

Asthma-associated genetic variants were obtained from the childhood-onset asthma genome-wide association study (GWAS) reported by Ferreira et al. (54). The GWAS summary statistics file was parsed to the Functional Mapping and Annotation (FUMA) platform (94), which uses PLINK to impute missing genotypes from the 1000 Genomes reference panel (95). Default settings were used, with the exception of $r^2$ (adapted to $r^2 < 0.8$). Genomic locations of the resulting SNPs were converted from GRCh37/hg19 to GRCh38/hg38 coordinates using the LiftOver tool of the UCSC Genome Browser (96). BEDTools' fisher command was used to calculate overlap between genomic features and candidate causal asthma SNPs.

### In situ Hi-C library preparation and initial data processing

In situ Hi-C was performed as previously described (68, 97) using ~200,000 human T cells as starting material. Libraries were sequenced on HiSeq 2500 sequencers (Illumina, paired-end, 75-bp read length) to a sequencing depth of >1.2 billion read pairs per T cell subset and activation state. Hi-C data were processed using an in-house pipeline based on TADbit (98) as previously described (68, 97). In brief, after trimming and removing poor quality reads, contact pairs were mapped using a fragment-based strategy as implemented in TADbit. Mapped reads were filtered to remove non-informative contacts (e.g., self-circle, dangling-end, PCR duplicates). Contact matrices obtained were normalized for sequencing depth and genomic biases using OneD (99). For differential interaction analysis and visualization, the resulting normalized matrices were directly subtracted.

### Identification of subnuclear compartments and TADs

To segment the genome into A/B compartments, we used Cscore-Tool (100) at 10-kb resolution, with computed C-scores reflecting quantitative association with A (0 to 1) or B (−1 to 0) compartments for each bin. Normalized contact matrices at 50-kb resolution were used to define TADs, using the previously described insulation score method (101) with default parameters. This procedure resulted in a set of borders (i.e., local minima in insulation score) for each replicate. Across replicates, overlapping borders or borders differing by only one bin were merged to obtain a list of reproducible borders for each T cell subset and activation state. Borders overlapping or differing in location by only one bin in all four experimental groups were considered common, and the rest were considered dynamic.

### Inter- and intracompartment strength measurements

Cooltools (10.5281/zenodo.5214125) was used to quantitatively segment the genome into A/B compartments on the basis of the first component of a PCA (PC1/EV1) on each of the normalized Hi-C matrices. AT content was used to assign negative and positive PC1 categories to the correct compartments. We based our analysis on the top 20% 100-kb bins showing the most extreme positive (A) or negative (B) PC1 values. We classified each bin in the genome according to PC1 percentiles and gathered contacts between each category, computing saddle strength profiles and generating saddle plots on the genomic bins.

### Clustering analysis of genome-wide C-score or TAD border insulation score dynamics

For A/B compartmentalization, average C-scores per bin per experimental group were calculated. Dynamic bins were identified as bins that exhibited a $\Delta$C-score > 0.3 in at least one pairwise comparison among our four experimental groups. Dynamic bins were grouped into 30 clusters using Mfuzz. We selected six recall-associated clusters on the basis of the average C-score of all bins in a cluster meeting the following criteria: memory $T_H2^-$ > naive$^-$, naive$^+$ > naive$^-$, and memory $T_H2^+$ > memory $T_H2^-$ (total $n = 11,874$ bins). Next, we selected bins within these clusters where the $\Delta$C-score between memory $T_H2^-$ and naive$^-$ was >0.15 ($n = 6888$ bins). Consecutive bins were merged into larger regions, and because we do not expect single bins to follow certain dynamics without neighboring bins following similar trajectories, single bins remaining after merging were excluded. Merged regions ($n = 754$ regions of >10 kb) were linked to genes on the basis of intersecting TSSs (RefSeq) and the GREAT annotations of the ATAC-Seq peaks described above. Insulation scores for all dynamic TAD borders ($n = 1463$) were averaged across replicates and subjected to clustering using Mfuzz, with recall-associated dynamics selected on the basis of visual inspection of clusters.

### Long-range interactions between ATAC-Seq peaks

Long-range interactions (2- to 10-Mb window) between ATAC-Seq peaks (from 10-kb resolution Hi-C matrices) were computed using the hicAggregateContacts command from HiCExplorer (102).

### Chromatin loop detection and meta-analysis of loops

Hi-C matrices at 5-kb resolution were converted to a cool format using HiCExplorer and parsed to Mustache (51) for chromatin loop detection using default parameters. Genome-wide aggregate plots (pile-ups of normalized signals at 5-kb resolution) of loops were generated with coolpup.py (103). Signals were plotted as heatmaps ranging from −50 to +50 kb of the loop anchor coordinates.

### Statistical analyses

Statistical parameters are reported in the figures and/or figure legends. Differential gene expression or peak enrichment of individual genes and peaks was calculated with the Wald test corrected for multiple testing according to the Benjamini-Hochberg procedure through DESeq2. FDR < 0.1 was considered significant for RNA-Seq, and FDR < 0.05 was considered significant for ATAC-Seq.

Enrichment of TF motifs, SNPs, or ATAC peaks within genomic regions was calculated with Fisher's exact test. For comparisons of means between groups, two-sided Mann-Whitney $U$ tests or Benjamini-Hochberg–corrected Kruskal-Wallis tests were performed, with $P < 0.05$ considered significant.

## Supplementary Materials

**This PDF file includes:**
Supplementary Methods
Figs. S1 to S9
Tables S1 to S3

**Other Supplementary Material for this manuscript includes the following:**
Data files S1 to S4
MDAR Reproducibility Checklist

View/request a protocol for this paper from *Bio-protocol*.

## REFERENCES AND NOTES

1. D. D. Chaplin, Overview of the immune response. *J. Allergy Clin. Immunol.* **125**, S3–S23 (2010).
2. J. Zhu, H. Yamane, W. E. Paul, Differentiation of effector CD4 T cell populations. *Annu. Rev. Immunol.* **28**, 445–489 (2010).
3. G. Natoli, R. Ostuni, Adaptation and memory in immune responses. *Nat. Immunol.* **20**, 783–792 (2019).
4. F. Sallusto, A. Lanzavecchia, K. Araki, R. Ahmed, From vaccines to memory and back. *Immunity* **33**, 451–463 (2010).
5. R. Stadhouders, E. Lubberts, R. W. Hendriks, A cellular and molecular view of T helper 17 cell plasticity in autoimmunity. *J. Autoimmun.* **87**, 1–15 (2018).
6. H. Hammad, B. N. Lambrecht, The basic immunology of asthma. *Cell* **184**, 1469–1485 (2021).
7. K. Kokubo, A. Onodera, M. Kiuchi, K. Tsuji, K. Hirahara, T. Nakayama, Conventional and pathogenic T$_H$2 cells in inflammation, tissue repair, and fibrosis. *Front. Immunol.* **13**, 945063 (2022).
8. T. C. Voss, G. L. Hager, Dynamic regulation of transcriptional states by chromatin and transcription factors. *Nat. Rev. Genet.* **15**, 69–81 (2014).
9. F. Grosveld, J. van Staalduinen, R. Stadhouders, Transcriptional regulation by (super)enhancers: From discovery to mechanisms. *Annu. Rev. Genomics Hum. Genet.* **22**, 127–146 (2021).
10. R. Stadhouders, G. J. Filion, T. Graf, Transcription factors and 3D genome conformation in cell-fate decisions. *Nature* **569**, 345–354 (2019).
11. B. Bonev, G. Cavalli, Organization and function of the 3D genome. *Nat. Rev. Genet.* **17**, 661–678 (2016).
12. A. M. Oudelaar, D. R. Higgs, The relationship between genome structure and function. *Nat. Rev. Genet.* **22**, 154–168 (2021).
13. E. E. M. Furlong, M. Levine, Developmental enhancers and chromosome topology. *Science* **361**, 1341–1345 (2018).
14. S. Schoenfelder, P. Fraser, Long-range enhancer-promoter contacts in gene expression control. *Nat. Rev. Genet.* **20**, 437–455 (2019).
15. D. Calderon, M. L. T. Nguyen, A. Mezger, A. Kathiria, F. Müller, V. Nguyen, N. Lescano, B. Wu, J. Trombetta, J. V. Ribado, D. A. Knowles, Z. Gao, F. Blaeschke, A. V. Parent, T. D. Burt, M. S. Anderson, L. A. Criswell, W. J. Greenleaf, A. Marson, J. K. Pritchard, Landscape of stimulation-responsive chromatin across diverse human immune cells. *Nat. Genet.* **51**, 1494–1505 (2019).
16. B. Soskic, E. Cano-Gamez, D. J. Smyth, W. C. Rowan, N. Nakic, J. Esparza-Gordillo, L. Bossini-Castillo, D. F. Tough, C. G. C. Larminie, P. G. Bronson, D. Willé, G. Trynka, Chromatin activity at GWAS loci identifies T cell states driving complex immune diseases. *Nat. Genet.* **51**, 1486–1493 (2019).
17. R. E. Gate, C. S. Cheng, A. P. Aiden, A. Siba, M. Tabaka, D. Lituiev, I. Machol, M. G. Gordon, M. Subramaniam, M. Shamim, K. L. Hougen, I. Wortman, S. C. Huang, N. C. Durand, T. Feng, P. L. de Jager, H. Y. Chang, E. L. Aiden, C. Benoist, M. A. Beer, C. J. Ye, A. Regev, Genetic determinants of co-accessible chromatin regions in activated T cells across humans. *Nat. Genet.* **50**, 1140–1150 (2018).
18. J. Yang, A. McGovern, P. Martin, K. Duffus, X. Ge, P. Zarrineh, A. P. Morris, A. Adamson, P. Fraser, M. Rattray, S. Eyre, Analysis of chromatin organization and gene expression in T cells identifies functional genes for rheumatoid arthritis. *Nat. Commun.* **11**, 4402 (2020).
19. N. G. Bediaga, H. D. Coughlan, T. M. Johanson, A. L. Garnham, G. Naselli, J. Schröder, L. G. Fearnley, E. Bandala-Sanchez, R. S. Allan, G. K. Smyth, L. C. Harrison, Multi-level remodelling of chromatin underlying activation of human T cells. *Sci. Rep.* **11**, 528 (2021).
20. O. S. Burren, A. Rubio García, B. M. Javierre, D. B. Rainbow, J. Cairns, N. J. Cooper, J. J. Lambourne, E. Schofield, X. Castro Dopico, R. C. Ferreira, R. Coulson, F. Burden, S. P. Rowlston, K. Downes, S. W. Wingett, M. Frontini, W. H. Ouwehand, P. Fraser, M. Spivakov, J. A. Todd, L. S. Wicker, A. J. Cutler, C. Wallace, Chromosome contacts in activated T cells identify autoimmune disease candidate genes. *Genome Biol.* **18**, 165 (2017).
21. B. Lai, Q. Tang, W. Jin, G. Hu, D. Wangsa, K. Cui, B. Z. Stanton, G. Ren, Y. Ding, M. Zhao, S. Liu, J. Song, T. Ried, K. Zhao, Trac-looping measures genome structure and chromatin accessibility. *Nat. Methods* **15**, 741–747 (2018).
22. S. Cuartero, G. Stik, R. Stadhouders, Three-dimensional genome organization in immune cell fate and function. *Nat. Rev. Immunol.* **23**, 206–221 (2023).
23. M. R. Mumbach, A. T. Satpathy, E. A. Boyle, C. Dai, B. G. Gowen, S. W. Cho, M. L. Nguyen, A. J. Rubin, J. M. Granja, K. R. Kazane, Y. Wei, T. Nguyen, P. G. Greenside, M. R. Corces, J. Tycko, D. R. Simeonov, N. Suliman, R. Li, J. Xu, R. A. Flynn, A. Kundaje, P. A. Khavari, A. Marson, J. E. Corn, T. Quertermous, W. J. Greenleaf, H. Y. Chang, Enhancer connectome in primary human cells identifies target genes of disease-associated DNA elements. *Nat. Genet.* **49**, 1602–1612 (2017).
24. A. T. Satpathy, N. Saligrama, J. D. Buenrostro, Y. Wei, B. Wu, A. J. Rubin, J. M. Granja, C. A. Lareau, R. Li, Y. Qi, K. R. Parker, M. R. Mumbach, W. S. Serratelli, D. G. Gennert, A. N. Schep, M. R. Corces, M. S. Khodadoust, Y. H. Kim, P. A. Khavari, W. J. Greenleaf, M. M. Davis, H. Y. Chang, Transcript-indexed ATAC-seq for precision immune profiling. *Nat. Med.* **24**, 580–590 (2018).
25. J. R. Giles, S. Manne, E. Freilich, D. A. Oldridge, A. E. Baxter, S. George, Z. Chen, H. Huang, L. Chilukuri, M. Carberry, L. Giles, N. P. P. Weng, R. M. Young, C. H. June, L. M. Schuchter, R. K. Amaravadi, X. Xu, G. C. Karakousis, T. C. Mitchell, A. C. Huang, J. Shi, E. J. Wherry, Human epigenetic and transcriptional T cell differentiation atlas for identifying functional T cell-specific enhancers. *Immunity* **55**, 557–574.e7 (2022).
26. P. Durek, K. Nordström, G. Gasparoni, A. Salhab, C. Kressler, M. de Almeida, K. Bassler, T. Ulas, F. Schmidt, J. Xiong, P. Glažar, F. Klironomos, A. Sinha, S. Kinkley, X. Yang, L. Arrigoni, A. D. Amirabad, F. B. Ardakani, L. Feuerbach, O. Gorka, P. Ebert, F. Müller, N. Li, S. Frischbutter, S. Schlickeiser, C. Cendon, S. Fröhler, B. Felder, N. Gasparoni, C. D. Imbusch, B. Hutter, G. Zipprich, Y. Tauchmann, S. Reinke, G. Wassilew, U. Hoffmann, A. S. Richter, L. Sieverling; DEEP Consortium, H. D. Chang, U. Syrbe, U. Kalus, J. Eils, B. Brors, T. Manke, J. Ruland, T. Lengauer, N. Rajewsky, W. Chen, J. Dong, B. Sawitzki, H. R. Chung, P. Rosenstiel, M. H. Schulz, J. L. Schultze, A. Radbruch, J. Walter, A. Hamann, J. K. Polansky, Epigenomic profiling of human CD4$^+$ T cells supports a linear differentiation model and highlights molecular regulators of memory development. *Immunity* **45**, 1148–1161 (2016).
27. W. J. Tu, K. Hardy, C. R. Sutton, R. McCuaig, J. Li, J. Dunn, A. Tan, V. Brezar, M. Morris, G. Denyer, S. K. Lee, S. J. Turner, N. Seddiki, C. Smith, R. Khanna, S. Rao, Priming of transcriptional memory responses via the chromatin accessibility landscape in T cells. *Sci. Rep.* **7**, 44825 (2017).
28. A. Barski, S. Cuddapah, A. V. Kartashov, C. Liu, H. Imamichi, W. Yang, W. Peng, H. C. Lane, K. Zhao, Rapid recall ability of memory T cells is encoded in their epigenome. *Sci. Rep.* **7**, 39785 (2017).
29. S. L. Bevington, P. Cauchy, J. Piper, E. Bertrand, N. Lalli, R. C. Jarvis, L. N. Gilding, S. Ott, C. Bonifer, P. N. Cockerill, Inducible chromatin priming is associated with the establishment of immunological memory in T cells. *EMBO J.* **35**, 515–535 (2016).
30. N. P. Weng, Y. Araki, K. Subedi, The molecular basis of the memory T cell response: Differential gene expression and its epigenetic regulation. *Nat. Rev. Immunol.* **12**, 306–315 (2012).
31. S. L. Bevington, P. Cauchy, P. N. Cockerill, Chromatin priming elements establish immunological memory in T cells without activating transcription. *Bioessays* **39**, (2017).
32. D. F. Tough, I. Rioja, L. K. Modis, R. K. Prinjha, Epigenetic regulation of T cell memory: Recalling therapeutic implications. *Trends Immunol.* **41**, 29–45 (2020).
33. A. C. Mullen, A. S. Hutchins, F. A. High, H. W. Lee, K. J. Sykes, L. A. Chodosh, S. L. Reiner, Hlx is induced by and genetically interacts with T-bet to promote heritable T$_H$1 gene induction. *Nat. Immunol.* **3**, 652–658 (2002).
34. G. J. van der Windt, D. O'Sullivan, B. Everts, S. C.-C. Huang, M. D. Buck, J. D. Curtis, C.-H. Chang, A. M. Smith, T. Ai, B. Faubert, R. G. Jones, E. J. Pearce, E. L. Pearce, CD8 memory T cells have a bioenergetic advantage that underlies their rapid recall ability. *Proc. Natl. Acad. Sci. U.S.A.* **110**, 14336–14341 (2013).

35. W. Wang, J. Guo, D. Yu, P. J. Vorster, W. J. Chen, Y. Wu, A dichotomy in cortical actin and chemotactic actin activity between human memory and naive T cells contributes to their differential susceptibility to HIV-1 infection. *J. Biol. Chem.* **287**, 35455–35469 (2012).

36. D. Lara-Astiaso, A. Weiner, E. Lorenzo-Vivas, I. Zaretsky, D. A. Jaitin, E. David, H. Keren-Shaul, A. Mildner, D. Winter, S. Jung, N. Friedman, I. Amit, Immunogenetics. Chromatin state dynamics during blood formation. *Science* **345**, 943–949 (2014).

37. S. Heinz, C. E. Romanoski, C. Benner, C. K. Glass, The selection and function of cell type-specific enhancers. *Nat. Rev. Mol. Cell Biol.* **16**, 144–154 (2015).

38. Y. Colino-Sanguino, S. J. Clark, F. Valdes-Mora, The H2A.Z-nucleosome code in mammals: Emerging functions. *Trends Genet.* **38**, 273–289 (2022).

39. C. Schmidl, A. F. Rendeiro, N. C. Sheffield, C. Bock, ChIPmentation: Fast, robust, low-input ChIP-seq for histones and transcription factors. *Nat. Methods* **12**, 963–965 (2015).

40. J. G. Peeters, S. J. Vervoort, S. C. Tan, G. Mijnheer, S. de Roock, S. J. Vastert, E. E. S. Nieuwenhuis, F. van Wijk, B. J. Prakken, M. P. Creyghton, P. J. Coffer, M. Mokry, J. van Loosdregt, Inhibition of super-enhancer activity in autoinflammatory site-derived T cells reduces disease-associated gene expression. *Cell Rep.* **12**, 1986–1996 (2015).

41. Q. Shan, S. Zhu, X. Chen, J. Liu, S. Yuan, X. Li, W. Peng, H.-H. Xue, Tcf1-CTCF cooperativity shapes genomic architecture to promote CD8$^+$ T cell homeostasis. *Nat. Immunol.* **23**, 1222–1235 (2022).

42. I. Tindemans, N. Serafini, J. P. Di Santo, R. W. Hendriks, GATA-3 function in innate and adaptive immunity. *Immunity* **41**, 191–206 (2014).

43. A. Kanhere, A. Hertweck, U. Bhatia, M. R. Gökmen, E. Perucha, I. Jackson, G. M. Lord, R. G. Jenner, T-bet and GATA3 orchestrate $T_H1$ and $T_H2$ differentiation through lineage-specific targeting of distal regulatory elements. *Nat. Commun.* **3**, 1268 (2012).

44. M. Yukawa, S. Jagannathan, S. Vallabh, A. V. Kartashov, X. Chen, M. T. Weirauch, A. Barski, AP-1 activity induced by co-stimulation is required for chromatin opening during T cell activation. *J. Exp. Med.* **217**, e20182009 (2020).

45. Y. Aikawa, K. Morimoto, T. Yamamoto, H. Chaki, A. Hashiramoto, H. Narita, S. Hirono, S. Shiozawa, Treatment of arthritis with a selective inhibitor of c-Fos/activator protein-1. *Nat. Biotechnol.* **26**, 817–823 (2008).

46. I. C. Ho, D. Lo, L. H. Glimcher, c-maf promotes T helper cell type 2 ($T_H2$) and attenuates $T_H1$ differentiation by both interleukin 4-dependent and -independent mechanisms. *J. Exp. Med.* **188**, 1859–1866 (1998).

47. R. Stadhouders, B. W. S. Li, M. J. W. de Bruijn, A. Gomez, T. N. Rao, H. J. Fehling, W. F. J. van IJcken, A. I. Lim, J. P. di Santo, T. Graf, R. W. Hendriks, Epigenome analysis links gene regulatory elements in group 2 innate lymphocytes to asthma susceptibility. *J. Allergy Clin. Immunol.* **142**, 1793–1807 (2018).

48. L. Chen, D. B. Flies, Molecular mechanisms of T cell co-stimulation and co-inhibition. *Nat. Rev. Immunol.* **13**, 227–242 (2013).

49. N. Yusufova, A. Kloetgen, M. Teater, A. Osunsade, J. M. Camarillo, C. R. Chin, A. S. Doane, B. J. Venters, S. Portillo-Ledesma, J. Conway, J. M. Phillip, O. Elemento, D. W. Scott, W. Béguelin, J. D. Licht, N. L. Kelleher, L. M. Staudt, A. I. Skoultchi, M. C. Keogh, E. Apostolou, C. E. Mason, M. Imielinski, T. Schlick, Y. David, A. Tsirigos, C. D. Allis, A. A. Soshnev, E. Cesarman, A. M. Melnick, Histone H1 loss drives lymphoma by disrupting 3D chromatin architecture. *Nature* **589**, 299–305 (2021).

50. P. Hua, M. Badat, L. L. P. Hanssen, L. D. Hentges, N. Crump, D. J. Downes, D. M. Jeziorska, A. M. Oudelaar, R. Schwessinger, S. Taylor, T. A. Milne, J. R. Hughes, D. R. Higgs, J. O. J. Davies, Defining genome architecture at base-pair resolution. *Nature* **595**, 125–129 (2021).

51. A. Roayaei Ardakany, H. T. Gezer, S. Lonardi, F. Ay, Mustache: Multi-scale detection of chromatin loops from Hi-C and Micro-C maps using scale-space representation. *Genome Biol.* **21**, 256 (2020).

52. C. G. Spilianakis, R. A. Flavell, Long-range intrachromosomal interactions in the T helper type 2 cytokine locus. *Nat. Immunol.* **5**, 1017–1027 (2004).

53. G. Seumois, L. Chavez, A. Gerasimova, M. Lienhard, N. Omran, L. Kalinke, M. Vedanayagam, A. P. V. Ganesan, A. Chawla, R. Djukanović, K. M. Ansel, B. Peters, A. Rao, P. Vijayanand, Epigenomic analysis of primary human T cells reveals enhancers associated with $T_H2$ memory cell differentiation and asthma susceptibility. *Nat. Immunol.* **15**, 777–788 (2014).

54. M. A. R. Ferreira, R. Mathur, J. M. Vonk, A. Szwajda, B. Brumpton, R. Granell, B. K. Brew, V. Ullemar, Y. Lu, Y. Jiang; 23andMe Research Team; eQTLGen Consortium; BIOS Consortium, P. K. E. Magnusson, R. Karlsson, D. A. Hinds, L. Paternoster, G. H. Koppelman, C. Almqvist, Genetic architectures of childhood- and adult-onset asthma are partly distinct. *Am. J. Hum. Genet.* **104**, 665–684 (2019).

55. V. P. Zediak, J. B. Johnnidis, E. J. Wherry, S. L. Berger, Cutting edge: Persistently open chromatin at effector gene loci in resting memory CD8$^+$ T cells independent of transcriptional status. *J. Immunol.* **186**, 2705–2709 (2011).

56. M. Yamashita, R. Shinnakasu, Y. Nigo, M. Kimura, A. Hasegawa, M. Taniguchi, T. Nakayama, Interleukin (IL)-4-independent maintenance of histone modification of the IL-4 gene loci in memory $T_H2$ cells. *J. Biol. Chem.* **279**, 39454–39464 (2004).

57. F. Mirabella, E. W. Baxter, M. Boissinot, S. R. James, P. N. Cockerill, The human IL-3/granulocyte-macrophage colony-stimulating factor locus is epigenetically silent in immature thymocytes and is progressively activated during T cell development. *J. Immunol.* **184**, 3043–3054 (2010).

58. W. H. Light, J. Freaney, V. Sood, A. Thompson, A. D'Urso, C. M. Horvath, J. H. Brickner, A conserved role for human Nup98 in altering chromatin structure and promoting epigenetic transcriptional memory. *PLOS Biol.* **11**, e1001524 (2013).

59. P. Pascual-Garcia, B. Debo, J. R. Aleman, J. A. Talamas, Y. Lan, N. H. Nguyen, K. J. Won, M. Capelson, Metazoan nuclear pores provide a scaffold for poised genes and mediate induced enhancer-promoter contacts. *Mol. Cell* **66**, 63–76.e6 (2017).

60. M. Yamashita, K. Hirahara, R. Shinnakasu, H. Hosokawa, S. Norikane, M. Y. Kimura, A. Hasegawa, T. Nakayama, Crucial role of MLL for the maintenance of memory T helper type 2 cell responses. *Immunity* **24**, 611–622 (2006).

61. C. Imbratta, H. Hussein, F. Andris, G. Verdeil, c-MAF, a swiss army knife for tolerance in lymphocytes. *Front. Immunol.* **11**, 206 (2020).

62. P. Li, W. J. Leonard, Chromatin accessibility and interactions in the transcriptional regulation of T cells. *Front. Immunol.* **9**, 2738 (2018).

63. Q. Shan, S. S. Hu, S. Zhu, X. Chen, V. P. Badovinac, W. Peng, C. Zang, H. H. Xue, Tcf1 preprograms the mobilization of glycolysis in central memory CD8$^+$ T cells during recall responses. *Nat. Immunol.* **23**, 386–398 (2022).

64. S. L. Bevington, R. Fiancette, D. W. Gajdasik, P. Keane, J. K. Soley, C. M. Willis, D. J. L. Coleman, D. R. Withers, P. N. Cockerill, Stable epigenetic programming of effector and central memory CD4 T cells occurs within 7 days of antigen exposure in vivo. *Front. Immunol.* **12**, 642807 (2021).

65. S. L. Bevington, P. Keane, J. K. Soley, S. Tauch, D. W. Gajdasik, R. Fiancette, V. Matei-Rascu, C. M. Willis, D. R. Withers, P. N. Cockerill, IL-2/IL-7-inducible factors pioneer the path to T cell differentiation in advance of lineage-defining factors. *EMBO J.* **39**, e105220 (2020).

66. D. Pham, C. E. Moseley, M. Gao, D. Savic, C. J. Winstead, M. Sun, B. L. Kee, R. M. Myers, C. T. Weaver, R. D. Hatton, Batf pioneers the reorganization of chromatin in developing effector T cells via Ets1-dependent recruitment of Ctcf. *Cell Rep.* **29**, 1203–1220.e7 (2019).

67. W. Wang, A. Chandra, N. Goldman, S. Yoon, E. K. Ferrari, S. C. Nguyen, E. F. Joyce, G. Vahedi, TCF-1 promotes chromatin interactions across topologically associating domains in T cell progenitors. *Nat. Immunol.* **23**, 1052–1062 (2022).

68. G. Stik, E. Vidal, M. Barrero, S. Cuartero, M. Vila-Casadesús, J. Mendieta-Esteban, T. V. Tian, J. Choi, C. Berenguer, A. Abad, B. Borsari, F. le Dily, P. Cramer, M. A. Marti-Renom, R. Stadhouders, T. Graf, CTCF is dispensable for immune cell transdifferentiation but facilitates an acute inflammatory response. *Nat. Genet.* **52**, 655–661 (2020).

69. S. Cuartero, F. D. Weiss, G. Dharmalingam, Y. Guo, E. Ing-Simmons, S. Masella, I. Robles-Rebollo, X. Xiao, Y. F. Wang, I. Barozzi, D. Djeghloul, M. T. Amano, H. Niskanen, E. Petretto, R. D. Dowell, K. Tachibana, M. U. Kaikkonen, K. A. Nasmyth, B. Lenhard, G. Natoli, A. G. Fisher, M. Merkenschlager, Control of inducible gene expression links cohesin to hematopoietic progenitor self-renewal and differentiation. *Nat. Immunol.* **19**, 932–941 (2018).

70. B. R. Sabari, A. Dall'Agnese, R. A. Young, Biomolecular condensates in the nucleus. *Trends Biochem. Sci.* **45**, 961–977 (2020).

71. R. S. Akondy, M. Fitch, S. Edupuganti, S. Yang, H. T. Kissick, K. W. Li, B. A. Youngblood, H. A. Abdelsamed, D. J. McGuire, K. W. Cohen, G. Alexe, S. Nagar, M. M. McCausland, S. Gupta, P. Tata, W. N. Haining, M. J. McElrath, D. Zhang, B. Hu, W. J. Greenleaf, J. J. Goronzy, M. J. Mulligan, M. Hellerstein, R. Ahmed, Origin and differentiation of human memory CD8 T cells after vaccination. *Nature* **552**, 362–367 (2017).

72. Y. Nakata, A. C. Brignier, S. Jin, Y. Shen, S. I. Rudnick, M. Sugita, A. M. Gewirtz, c-Myb, Menin, GATA-3, and MLL form a dynamic transcription complex that plays a pivotal role in human T helper type 2 cell development. *Blood* **116**, 1280–1290 (2010).

73. T. Vierbuchen, E. Ling, C. J. Cowley, C. H. Couch, X. Wang, D. A. Harmin, C. W. M. Roberts, M. E. Greenberg, AP-1 transcription factors and the BAF complex mediate signal-dependent enhancer selection. *Mol. Cell* **68**, 1067–1082.e12 (2017).

74. M. E. Raeber, Y. Zurbuchen, D. Impellizzieri, O. Boyman, The role of cytokines in T-cell memory in health and disease. *Immunol. Rev.* **283**, 176–193 (2018).

75. W. Lai, M. Yu, M. N. Huang, F. Okoye, A. D. Keegan, D. L. Farber, Transcriptional control of rapid recall by memory CD4 T cells. *J. Immunol.* **187**, 133–140 (2011).

76. F. Salerno, S. Engels, M. van den Biggelaar, F. P. J. van Alphen, A. Guislain, W. Zhao, D. L. Hodge, S. E. Bell, J. P. Medema, M. von Lindern, M. Turner, H. A. Young, M. C. Wolkers, Translational repression of pre-formed cytokine-encoding mRNA prevents chronic activation of memory T cells. *Nat. Immunol.* **19**, 828–837 (2018).

77. D. L. Farber, Biochemical signaling pathways for memory T cell recall. *Semin. Immunol.* **21**, 84–91 (2009).

78. R. I. K. Geltink, R. L. Kyle, E. L. Pearce, Unraveling the complex interplay between T cell metabolism and function. *Annu. Rev. Immunol.* **36**, 461–488 (2018).

79. E. K. van der Ploeg, K. Golebski, M. van Nimwegen, J. R. Fergusson, B. A. Heesters, I. Martinez-Gonzalez, C. M. A. Kradolfer, S. van Tol, B. P. Scicluna, M. J. W. de Bruijn, G. M. de Boer, G. A. Tramper-Stranders, G. J. Braunstahl, W. F. J. van IJcken, A. P. Nagtegaal, C. M. van Drunen, W. J. Fokkens, D. Huylebroeck, H. Spits, R. W. Hendriks, R. Stadhouders, S. M. Bal, Steroid-resistant human inflammatory ILC2s are marked by CD45RO and elevated in type 2 respiratory diseases. *Sci. Immunol.* **6**, eabd3489 (2021).

80. I. Tindemans, H. Vroman, M. Lukkes, M. van Nimwegen, M. J. W. de Bruijn, B. W. S. Li, A. Kleinjan, G. M. de Boer, G. A. Tramper-Stranders, M. Kool, G. J. Braunstahl, R. W. Hendriks, Increased surface expression of NOTCH on memory T cells in peripheral blood from patients with asthma. *J. Allergy Clin. Immunol.* **143**, 769–771.e3 (2019).

81. S. Picelli, O. R. Faridani, Å. K. Björklund, G. Winberg, S. Sagasser, R. Sandberg, Full-length RNA-seq from single cells using Smart-seq2. *Nat. Protoc.* **9**, 171–181 (2014).

82. A. Seki, S. Rutz, Optimized RNP transfection for highly efficient CRISPR-Cas9–mediated gene knockout in primary T cells. *J. Exp. Med.* **215**, 985–997 (2018).

83. D. Kim, B. Langmead, S. L. Salzberg, HISAT: A fast spliced aligner with low memory requirements. *Nat. Methods* **12**, 357–360 (2015).

84. S. Heinz, C. Benner, N. Spann, E. Bertolino, Y. C. Lin, P. Laslo, J. X. Cheng, C. Murre, H. Singh, C. K. Glass, Simple combinations of lineage-determining transcription factors prime cis-regulatory elements required for macrophage and B cell identities. *Mol. Cell* **38**, 576–589 (2010).

85. M. I. Love, W. Huber, S. Anders, Moderated estimation of fold change and dispersion for RNA-seq data with DESeq2. *Genome Biol.* **15**, 550 (2014).

86. S. J. Lê, J. Josse, F. Husson, FactoMineR: A package for multivariate analysis. *J. Stat. Softw.* **25**, 1–18 (2008).

87. O. H. Hammer, D. A. T. Harper, P. D. Ryan, PAST: Paleontological statistics software package for education and data analysis. *Palaeontol. Electron.* **4**, 1–9 (2001).

88. Y. Zhou, B. Zhou, L. Pache, M. Chang, A. H. Khodabakhshi, O. Tanaseichuk, C. Benner, S. K. Chanda, Metascape provides a biologist-oriented resource for the analysis of systems-level datasets. *Nat. Commun.* **10**, 1523 (2019).

89. H. Li, B. Handsaker, A. Wysoker, T. Fennell, J. Ruan, N. Homer, G. Marth, G. Abecasis, R. Durbin; 1000 Genome Project Data Processing Subgroup, The sequence alignment/map format and SAMtools. *Bioinformatics* **25**, 2078–2079 (2009).

90. J. T. Robinson, H. Thorvaldsdóttir, W. Winckler, M. Guttman, E. S. Lander, G. Getz, J. P. Mesirov, Integrative genomics viewer. *Nat. Biotechnol.* **29**, 24–26 (2011).

91. C. Y. McLean, D. Bristor, M. Hiller, S. L. Clarke, B. T. Schaar, C. B. Lowe, A. M. Wenger, G. Bejerano, GREAT improves functional interpretation of cis-regulatory regions. *Nat. Biotechnol.* **28**, 495–501 (2010).

92. M. E. Futschik, B. Carlisle, Noise-robust soft clustering of gene expression time-course data. *J. Bioinform. Comput. Biol.* **3**, 965–988 (2005).

93. A. R. Quinlan, I. M. Hall, BEDTools: A flexible suite of utilities for comparing genomic features. *Bioinformatics* **26**, 841–842 (2010).

94. K. Watanabe, E. Taskesen, A. van Bochoven, D. Posthuma, Functional mapping and annotation of genetic associations with FUMA. *Nat. Commun.* **8**, 1826 (2017).

95. S. Purcell, B. Neale, K. Todd-Brown, L. Thomas, M. A. R. Ferreira, D. Bender, J. Maller, P. Sklar, P. I. W. de Bakker, M. J. Daly, P. C. Sham, PLINK: A tool set for whole-genome association and population-based linkage analyses. *Am. J. Hum. Genet.* **81**, 559–575 (2007).

96. A. S. Hinrichs, D. Karolchik, R. Baertsch, G. P. Barber, G. Bejerano, H. Clawson, M. Diekhans, T. S. Furey, R. A. Harte, F. Hsu, J. Hillman-Jackson, R. M. Kuhn, J. S. Pedersen, A. Pohl, B. J. Raney, K. R. Rosenbloom, A. Siepel, K. E. Smith, C. W. Sugnet, A. Sultan-Qurraie, D. J. Thomas, H. Trumbower, R. J. Weber, M. Weirauch, A. S. Zweig, D. Haussler, W. J. Kent, The UCSC genome browser database: Update 2006. *Nucleic Acids Res.* **34**, D590–D598 (2006).

97. R. Stadhouders, E. Vidal, F. Serra, B. di Stefano, F. le Dily, J. Quilez, A. Gomez, S. Collombet, C. Berenguer, Y. Cuartero, J. Hecht, G. J. Filion, M. Beato, M. A. Marti-Renom, T. Graf, Transcription factors orchestrate dynamic interplay between genome topology and gene regulation during cell reprogramming. *Nat. Genet.* **50**, 238–249 (2018).

98. F. Serra, D. Baù, M. Goodstadt, D. Castillo, G. J. Filion, M. A. Marti-Renom, Automatic analysis and 3D-modelling of Hi-C data using TADbit reveals structural features of the fly chromatin colors. *PLOS Comput. Biol.* **13**, e1005665 (2017).

99. E. Vidal, F. le Dily, J. Quilez, R. Stadhouders, Y. Cuartero, T. Graf, M. A. Marti-Renom, M. Beato, G. J. Filion, OneD: Increasing reproducibility of Hi-C samples with abnormal karyotypes. *Nucleic Acids Res.* **46**, e49 (2018).

100. X. Zheng, Y. Zheng, CscoreTool: Fast Hi-C compartment analysis at high resolution. *Bioinformatics* **34**, 1568–1570 (2018).

101. E. Crane, Q. Bian, R. P. McCord, B. R. Lajoie, B. S. Wheeler, E. J. Ralston, S. Uzawa, J. Dekker, B. J. Meyer, Condensin-driven remodelling of X chromosome topology during dosage compensation. *Nature* **523**, 240–244 (2015).

102. F. Ramirez, V. Bhardwaj, L. Arrigoni, K. C. Lam, B. A. Grüning, J. Villaveces, B. Habermann, A. Akhtar, T. Manke, High-resolution TADs reveal DNA sequences underlying genome organization in flies. *Nat. Commun.* **9**, 189 (2018).

103. I. M. Flyamer, R. S. Illingworth, W. A. Bickmore, *Coolpup.py:* Versatile pile-up analysis of Hi-C data. *Bioinformatics* **36**, 2980–2985 (2020).

104. THE ENCODE Project Consortium, An integrated encyclopedia of DNA elements in the human genome. *Nature* **489**, 57–74 (2012).

# Science Immunology

## 3D chromatin reprogramming primes human memory T$_H$2 cells for rapid recall and pathogenic dysfunction

Anne Onrust-van Schoonhoven, Marjolein J.W. de Bruijn, Bernard Stikker, Rutger W.W. Brouwer, Gert-Jan Braunstahl, Wilfred F.J. van IJcken, Thomas Graf, Danny Huylebroeck, Rudi W. Hendriks, Grgoire Stik, and Ralph Stadhouders

**Editor's summary**

Long-lived memory T cells provide immunological protection by rapidly responding upon antigen re-encounter, but they can also contribute to disease by causing excessive inflammation. Using multi-scale epigenomics, Onrust-van Schoonhoven *et al.* examined how the three-dimensional organization of chromatin facilitates rapid recall of human memory T helper 2 (T$_H$2) cells. By systematically comparing primary memory T$_H$2 and naïve T cells, they identified specific gene expression modules linked to recall response that were already epigenomically primed before restimulation. Transcriptional priming occurred through organization of recall genes with their enhancers in specific topological structures that facilitated activation by AP-1 transcription factor. Memory T$_H$2 cells from patients with severe asthma displayed excessive priming of recall genes, including at genetic susceptibility loci, suggesting that epigenomic reprogramming could contribute to pathogenic T$_H$2 responses. —Claire Olingy

**View the article online**
https://www.science.org/doi/10.1126/sciimmunol.adg3917
**Permissions**
https://www.science.org/help/reprints-and-permissions

Use of this article is subject to the Terms of service